ApJ, 486, in press

On the Origin of the UV Upturn in Elliptical Galaxies. I. Sensitivity of UV Population Synthesis to Various Input Parameters

Sukyoung Yi[1]
Department of Astronomy, Yale University, P.O. Box 208101, New Haven, CT 06520-8101,
NASA/Goddard Space Flight Center, Code 681, Greenbelt, MD 20771
email: yi@shemesh.gsfc.nasa.gov

Pierre Demarque and Augustus Oemler, Jr.[2]
Department of Astronomy, Yale University, P.O. Box 208101, New Haven, CT 06520-8101
demarque@astro.yale.edu oemler@ociw.edu

ABSTRACT

We present models of the late stages of stellar evolution intended to explain the "UV upturn" phenomenon in elliptical galaxies. Such models are sensitive to values of a number of poorly-constrained physical parameters, including metallicity, age, stellar mass loss, helium enrichment, and the distribution of stars on the zero age horizontal branch (HB). We explore the sensitivity of the results to values of these parameters, and reach the following conclusions.

Old, metal rich galaxies, such as giant ellipticals, naturally develop a UV upturn within a reasonable time scale - less than a Hubble time - without the presence of young stars. The most likely stars to dominate the UV flux of such populations are low mass, core helium burning (HB and evolved HB) stars. Metal-poor populations produce a higher ratio of UV-to-V flux, due to opacity effects, but only metal-rich stars develop a UV upturn, in which the flux increases towards shorter UV wavelengths.

Model color-magnitude diagrams and corresponding integrated spectra (for various values of age, metallicity, helium enrichment, mass loss efficiency, initial mass function, and the HB mass dispersion factor) are available on S.Y.'s world wide web site http://shemesh.gsfc.nasa.gov/model.html.

Subject headings: galaxies: elliptical and lenticular, cD - galaxies: evolution - galaxies: stellar content - ultraviolet: galaxies

---

[1]National Research Council Research Associate.

[2]Also at Carnegie Observatories, 813 Santa Barbara St., Pasadena, CA 91101

1. Introduction

The evolutionary population synthesis (EPS) technique, first introduced by Tinsley (1968; see Tinsley 1980 and Bruzual & Charlot 1993 for review), has its fundamental basis in stellar evolution theory. Unlike the static population synthesis[3] technique (e.g. McClure & van den Bergh 1968; Spinrad & Taylor 1971; Faber 1972; O'Connell 1976; Pickles 1985b; see O'Connell 1987 for review) that adopts physical constraints from the observational data, EPS relies on theoretical constraints, most importantly the evolutionary time scale of stars.

Some significant advantages of EPS include the following: (1) the theoretical results can provide physical understanding *when* the results fit the observations reasonably because the solution is unique, (2) it allows us to understand not only the present observable quantities but also the evolution of those quantities, (3) it is easy to implement the theoretical predictions into the code, and (4) it is easier to investigate the sensitivity of the result to input assumptions that are used in the modeling. While aspects (1) and (2) have been widely recognized, the significance of aspects (3) and (4) is still poorly understood.

As an example of aspect (3), EPS enables us to include hypothetical stars that are predicted to exist and significant contributors to the integrated flux but rarely observed. For instance, several stellar evolution theory groups have predicted that, under certain conditions, low mass core helium-burning stars (horizontal branch - HB - stars) become UV-bright before they become white dwarf (WD) stars (Demarque & Pinsonneault 1988; Greggio & Renzini 1990; Castellani & Tornambé 1991; Horch, Demarque, & Pinsonneault 1992). These UV-bright stars, the so-called slow blue phase (SBP) stars (Horch et al. 1992) which include both AGB-manqué stars (Greggio & Renzini 1990) and post-early-AGB (PEAGB, Castellani & Tornambé 1991) stars, can be realistically taken into account only through the EPS technique. Yi, Demarque, & Kim (1997, hereafter YDK) provided a detailed physical description of the UV-bright phase.

On the other hand, the reliability of EPS is restricted by uncertainty in the stellar physics. The SBP stars give an example again. They were unknown until recently. Thus, early EPS studies were not able to include them, despite their probable significance in the UV study. However, such pure theoretical predictions from stellar astrophysics may not be realistic: such stars may not exist. Then, the EPS using such theoretical constraints would result in wrong conclusions. Therefore, in earlier times when many of the stellar evolutionary phenomena other than the main sequence (MS) and red giant branch (RGB) were unclear, the static population synthesis technique was more popular.

However, there has been remarkable progress in the advanced stellar evolution theory during the past few decades, especially for the core helium-burning phase (e.g. Rood 1973; Sweigart, Mengel, & Demarque 1974; Sweigart 1987; Lee & Demarque 1990; Castellani & Tornambé 1991;

[3]Alternatively, "optimized (or optimizing) synthesis" (O'Connell 1987).

Horch et al. 1992; Dorman, Rood, & O'Connell 1993; Fagotto et al. 1994; YDK). Therefore, many groups are now including advanced phases of stellar evolution in EPS (e.g. Nesci & Perola 1985; Magris & Bruzual 1993; Bressan, Chiosi, & Fagotto 1994; Buzzoni 1995; Dorman, O'Connell, & Rood 1995; Yi et al. 1995; Park & Lee 1997). Many of them are mainly aiming at solving the "UV upturn problem", where the UV upturn is defined as the increasing flux in the UV (1,000 – 2,500 Å) with decreasing wavelength, as found in giant elliptical galaxies (Code & Welch 1979; Faber 1983; Burstein et al. 1988).

The most serious concern about such elaborate population studies is that the effects of input parameters on the resulting UV flux are very poorly understood. Unlike population synthesis in the optical band, UV population synthesis for old stellar systems, such as elliptical galaxies, is very sensitive to various detailed physical assumptions. This is because most candidates for UV sources are highly evolved stars whose properties are governed by several input parameters that have not yet been determined very well. Among such parameters are mass loss and its distribution, galactic helium enrichment ($\Delta Y/\Delta Z$), and initial mass function. In particular, as we will show later, the assumptions about mass loss and its distribution influence the magnitude of the resulting UV flux significantly. Many recent population synthesis studies have been presented to the readers without addressing the sensitivity of their results and conclusions to alterations in the adopted input parameters.

The main goals of this paper are to illustrate the sensitivity of the model UV spectrum to various input parameters, and to investigate the plausibility of UV-bright core helium-burning stars as the major UV sources in giant elliptical galaxies. This paper complements previous works in the literature. Greggio & Renzini (1990) explored the sensitivity of the UV modeling to $\Delta Y/\Delta Z$ and to the metallicity-dependence of mass loss. The effects of age and metallicity have been investigated by several groups, among which the works of Bressan et al. (1994), Dorman et al. (1995), and Tantalo et al. (1996) are noteworthy. Although these groups and others (most notably the empirical works done by the HUT team; Ferguson & Davidsen 1993; Brown et al. 1997) have tested the plausibility of core helium-burning stars as the main UV sources in giant elliptical galaxies before, we found it necessary to investigate it within a fuller parameter space, in those cases where several input parameters' influence are still poorly known.

Realistic synthetic HB, based on gaussian mass dispersion on the HB, has been used in our population synthesis. Although Park & Lee (1997) used the same technique in their recent study for the first time, ours is the first to combine the mass loss as a function of age and metallicity and gaussian mass dispersion. We will show why realistic HB treatment is important. We also would like to demonstrate that intricate astrophysics must be considered in estimating mass loss and in incorporating the estimates into the population synthesis code, even for the most simplistic approach (e.g. Reimers' mass loss formula).

In order to distinguish the effects of these input parameters from others, all the models in this paper are based on simple model populations in which all stars are born at the same time with

the same chemical composition. *This study focuses on the sensitivity of the UV modeling to the adopted input parameters, and, thus, does not include a detailed comparison between models and observational data.* The following paper (Yi, Demarque, & Oemler 1997) in the series is mainly dedicated to such comparisons.

2. Stellar Spectral Library Construction

An obvious source of uncertainty in EPS is the stellar spectral library used to convert the theoretical quantities (such as $T_{\rm eff}$, $\log g$, and radius R) into observable ones (e.g. magnitudes, colors and spectral line strengths) (Charlot, Worthey, & Bressan 1996). Galaxy models have been based on either empirical stellar spectral libraries which are highly incomplete in the super metal-rich ($Z > Z_{\odot}$) regime and lack UV data, or on theoretical libraries that do not reproduce observed stellar spectra precisely, and have not been fully verified empirically at UV wavelengths.

There are several comprehensive empirical libraries (e.g. Gunn & Stryker 1983; Pickles 1985a; Silva & Cornell 1992) in the optical through near-infrared (IR) bands, and they have been used in many population synthesis studies. In general, they are adequate for MS through RGB stars and in the solar abundance regime. However, elliptical galaxies are believed to be metal-rich, and no adequate empirical library exists for super metal-rich ($Z > Z_{\odot}$) stars. In particular, the lack of empirical spectra of evolved, metal-rich stars, such as SBP (slow blue phase) stars, is a serious drawback for UV studies. The best UV spectral library is derived from IUE observations (Fanelli, O'Connell, & Thuan 1987; Fanelli et al. 1992); however, it lacks super metal-rich ($> Z_{\odot}$) samples, and does not cover the far UV near the *Lyman* limit that is crucial to the UV upturn study.

On the other hand, theoretical spectral libraries suffer from insufficient atomic data and physical understanding. Even the most recent models may be inadequate, especially for cool stars (Buser & Kurucz 1992; Morossi et al. 1993; Kirkpatrick et al. 1993; Gustafsson & Jørgensen 1994). These theoretical libraries have to be validated by acquiring as much empirical data as possible. But, the validation in the UV wavelength is possible only using the space facilities which have limited and competitive observing time.

While both empirical and theoretical libraries have problems, a great advantage of using the theoretical spectral library is that we can clearly see the effects of various parameters, such as temperature, metallicity, and surface gravity, in the models. Moreover, the recent Kurucz library covers the high metallicities and high temperatures that are crucial to highly evolved stars and thus to UV studies, but that are not available empirically. Thus, a theoretical library has been chosen, assuming that the uncertainty in the model spectra is still smaller than the effects of temperature and metallicity that cannot be studied adequately using empirical libraries.

The foundation of the spectral library in this study is the Kurucz library (1992). It covers $[Fe/H] = -4$ – $+1$, $T_{\rm eff} = 3{,}500$ – $50{,}000$ K, and $\log g = 0.0$ – 5.0 (see Kurucz (1992) for details of the grids). Additional spectra have been constructed for the stars with high $T_{\rm eff}$ and/or high

$\log g$ using the 1995 version of the Hubeny spectral synthesis code, TLUSTY178 (see Hubeny 1988 for details). The effects of $T_{\rm eff}$ and metallicity are demonstrated in Figures 1 – 2.

Since the metallicity effects are small when $T_{\rm eff} \gtrsim$ 50,000 K, all models for $T_{\rm eff} >$ 50,000 K have been constructed for $Z = Z_{\odot}$. The stellar spectrum for each star is constructed using linear interpolation in metallicity and surface gravity. However, for $T_{\rm eff}$, the population synthesis code finds the model spectrum with the closest temperature in the library instead of interpolating in the temperature grid in order to save CPU time. For example, the code will use model spectra of $T_{\rm eff}$ = 3,500 K and 3,750 K for the stars of $T_{\rm eff}$ = 3,400 K and 3,650 K. This approach slightly overestimates the contribution from such cool stars in the composite spectrum in the IR because the minimum $T_{\rm eff}$ in the Kurucz library is 3,500 K. However, this effect is negligible in the UV and optical range because only a small number of stars are that cool and such cool stars contribute little to the integrated light in the UV to optical range.

3. Construction of synthetic CMDs and SEDs

EPS consists of two steps, constructing model color-magnitude diagrams (CMDs) and spectral energy distributions (SEDs). It will be shown later in this study that a careful synthetic CMD construction including a realistic HB is crucial, especially for UV population synthesis. The model CMD provides basic information, such as $[Fe/H]$, $T_{\rm eff}$, $\log g$, and the radius of the star R. Since a model stellar spectrum is defined only by $[Fe/H]$, $T_{\rm eff}$, $\log g$, and R, i.e.

$$f_{\lambda} \, = \, f([Fe/H],\, T_{eff},\, \log\, g,\, R), \tag{1}$$

the convolution of this information with the spectral library generates a model composite spectrum.

The core helium-burning phase in the population synthesis requires a complicated treatment involving a synthetic HB construction. Therefore the core hydrogen-burning phase (MS and RGB) and the core helium-burning phase - strictly speaking, post-RGB: HB, asymptotic giant branch (AGB), slow blue phase (SBP), post-AGB (PAGB), and white dwarf (WD) - have been dealt with separately. Then, the total flux F_{λ} is the sum of the flux from the core hydrogen-burning stars F_{λ}^{H} and that from the core helium-burning stars F_{λ}^{He}

$$F_{\lambda} \, = \, F_{\lambda}^{H} \, + \, F_{\lambda}^{He}. \tag{2}$$

The foundations of the model CMD construction are the Yale Isochrones 1996 (Demarque et al. 1996) and Yi et al.'s post-RGB tracks (YDK).

3.1. Core hydrogen-burning phase: MS and RGB

The core hydrogen-burning phase is relatively easier to deal with because both MS and RGB are well understood. The Yale Isochrones 1996 provides all the necessary information of the core-hydrogen burning stars for the population synthesis.

The initial mass function (IMF) is assumed to follow a conventional power law as follows,

$$\frac{d\,n_i}{d\,M_i} = \alpha\, M_i^{-(x+1)} \tag{3}$$

where M_i is the stellar mass, n_i is the number of stars in the ith mass bin, α is a normalization constant, and x is the IMF slope. Three values of x, namely -1, 1.35, and 3, are chosen to see the effects of IMF on the model CMDs and SEDs; the models with $x = 1.35$ (Salpeter 1955; Larson 1992; Larson 1995) are considered to be standard.

The flux from all the core hydrogen-burning stars, on the MS and RGB, F_λ^H, is

$$F_\lambda^H = \sum_i n_i\ f_{\lambda,i} \tag{4}$$

where

$$n_i = \alpha \int_{M_i-\delta M}^{M_i+\delta M} M^{-(x+1)}\, dM. \tag{5}$$

The normalization constant α has been set to make the mass of the model galaxy $10^{12}\ M_\odot$. This large number avoids any stochastic effect from rare bright stars. One of the nice features of the population synthesis of giant elliptical galaxies is that giant elliptical galaxies are composed of a sufficiently large number of stars that we can avoid a serious stochastic effect where statistical fluctuations of a few bright stars can influence the SED. On the contrary, population synthesis for small galaxies and star clusters suffers from the stochastic effect. Therefore, such studies must be approached with caution.

3.2. Mass loss estimation

Mass loss is one of the most important, but least understood processes in stellar astrophysics. It has a dominant influence on the UV evolution of galaxies because the mass loss determines the mean $T_{\rm eff}$ of core helium-burning stars that are the major UV sources in old stellar systems, as will be shown later.

Reimers' empirical formula of mass loss (Reimers 1975)

$$\frac{dM}{dt} = -4\ \times\ 10^{-13}\,\eta\,\frac{L}{g\,R}, \tag{6}$$

where L is the luminosity, g is the surface gravity, and R is the radius, has been used in this study. The mass loss efficiency parameter, η, an empirical fitting factor, was originally chosen to be unity

based on the study of 16 metal-rich (Population I) red giant stars (Reimers 1975). However, η has been reported to vary remarkably from 0.25 to 2 – 3 (Dupree 1986; Kudritzki & Reimers 1978; Renzini 1981). While the estimated η for metal-rich stars varies significantly, the estimated range of η for metal-poor stars seems to be much better determined. Most studies on metal-poor stars suggest $\eta = 0.3 - 0.6$ (Aaronson & Mould 1982; Mould & Aaronson 1982; Renzini 1981; Lee, Demarque, & Zinn 1994).

One of the best ways to estimate the mass loss in metal-poor stars uses the fact that the mass of the RR Lyrae variables (a type of HB star) and the mass of the red giants can be determined independently. In principle, the mass loss on the RGB can be deduced from the mass difference between red giants and HB stars. However, a precise, empirical mass estimation of ordinary HB stars is difficult to achieve. Several pulsation studies showed that the mass of a particular type of RR Lyrae stars (RR-d double mode variables) can be reasonably estimated (Petersen 1973). The mass of RR Lyrae stars can also be measured via stellar evolution theory by fitting the observed HB morphology with synthetic HBs (Yi, Lee, & Demarque 1993). For a long time, there existed an inconsistency between the evolutionary mass of RR Lyrae variables and their pulsation mass, in the sense that the pulsation masses were lower (Petersen 1973; Lee, Demarque & Zinn 1990). This discrepancy raised doubts in the minds of many variable star researchers about the validity of the HB evolutionary models (e.g. Clement, Kinman, & Suntzeff 1991). Accordingly, the true mass loss on the RGB was unclear. However, the mass estimates from the two independent methods are now in good agreement when improved physics including the OPAL opacities is used (Kovacs, Buchler, & Marom 1991; Cox 1991; Yi et al. 1993)[4]. Because of this agreement, we can reasonably estimate the amount of mass loss experienced by the red giant progenitors of double mode RR Lyrae stars, once the masses of red giants are provided. The masses of the red giants as a function of age and chemical composition can be reliably deduced from the stellar evolution theory.

In order to redetermine η for metal-poor stars in this study, we adopted the evolutionary mass of RR Lyrae stars in metal-poor globular clusters, M15 ($Z = 0.0001$) and M3 ($Z = 0.0004$), from Yi et al. (1993) and the mass of red giants from the Yale Isochrones 1996. It should be emphasized that η estimation based on the HB morphology, that is, on the mass estimates of RR Lyrae stars, must use the new mass estimates of RR Lyrae stars after the RR Lyrae mass discrepancy has been removed. If the old, lower mass is used, the η would be overestimated by almost a factor of two.

The mass loss (Table 1 – 4) has been calculated using Reimers' formula which is applied to MS – RGB stellar evolutionary tracks that have been constructed without mass loss. Several evolutionary tracks of different masses were selected for the mass loss estimation in order to

[4] There still may be inconsistency in the estimated masses of HB stars. Recent spectral analyses (e.g. Moehler, Heber, & de Boer 1995; de Boer, Tucholke, & Schmidt 1997) of hot stars on the blue tail of M 15 report that the mass estimation is substantially lower than what canonical HB models suggest, raising a question either about the origin of the hot stars on the blue tail or the validity of stellar evolutionary calculations. On the other hand, de Boer et al. note that "the likely cause for the discrepancy of the mass values lies in the low gravities derived from Balmer line profiles." (see also Cacciari et al. 1995)

approximately cover the range of 1 – 25 Gyr of age. For example, in the case of $Z = 0.02$ ($\approx Z_{\odot}$), the tracks of 1.8 $M_{\odot}$ (lifetime on the MS – RGB $\approx$ 1.3 Gyr), 1.4 $M_{\odot}$ (3.3 Gyr), 1.0 $M_{\odot}$ (11.1 Gyr), and 0.8 $M_{\odot}$ (31.5 Gyr) were used to estimate the mass loss at 1.3, 3.3, 11.1, and 31.5 Gyr, and linear interpolation was carried out within this age range. Therefore, in a 10 billion years old stellar system with (Z, Y) = (0.02, 0.27) where most stars on the MS through RGB are slightly heavier than $1.0M_{\odot}$, Reimers' formula suggests that stars experience mass loss of about 0.119 (if $\eta = 0.3$) – 0.396 $M_{\odot}$ (if $\eta = 1.0$) (see the second top left panel in Figure 4 and Table 1 – 4) depending on the adopted η. We assume the mass loss becomes noticeable when $L \geq L_{\odot}$. Also, the mass loss has been forced to stop in the numerical calculations either when the star reaches the helium core flash stage or when it causes the envelope mass M_{env} to be smaller than 0.01 $M_{\odot}$ (as the star loses mass and as the core mass M_{core} grows).

It has been suggested that M_{env} cannot be infinitesimally small (Sweigart et al. 1974) for the following reason. A certain mass is required to be present in the stellar envelope in order to exert sufficient gravitational pressure on the degenerate core of an RGB star and to cause a helium core flash (we call this *the minimum M_{env} hypothesis*). This is how HB stars are born. It is believed that nearly all the energy produced by the helium core flash is consumed in removing the degeneracy of the core and that there is not enough energy to expel any significant amount of envelope material into space (Tomasko 1970; Cole & Deupree 1980; Cole, Demarque, & Deupree 1985). The minimum M_{env} has been suggested to be approximately 0.01 – 0.02 $M_{\odot}$ (Hayashi, Hoshi, & Sugimoto 1962; Refsdal & Weigert 1970; Sweigart et al. 1974).

However, it is still debatable whether such a minimum M_{env} exists considering that there are hot (low-mass) field subdwarf stars (see Sweigart et al. 1974 for review) and low-mass UV-bright stars in NGC 6791 (Kaluzny & Udalski 1992; Liebert, Saffer, & Green 1994; Kaluzny & Rucinski 1995) that seem to have an envelope of $M_{env} \lesssim 0.01\ M_{\odot}$. In particular, D'Cruz et al. (1996) recently suggested that such a minimum M_{env} does not exist. Instead, they claimed that red giants with a very smaller envelope mass experience helium-core flash after leaving the tip of the RGB quietly. We do not include such models in this paper, but we believe that their finding is quite plausible and deserves further investigations both to verify it with thorough theoretical calculations and to explore the effect of it to the population synthesis. While the value of the minimum M_{env} is not yet clear, 0.01 $M_{\odot}$ has been chosen in this study in order to approximately accommodate the hot stars in NGC 6791 and the hot field subdwarf stars.

Much of the mass loss is believed to occur during the bright phase of the RGB because it is sensitive to the stellar radius R, and R increases dramatically as a red giant evolves along the RGB. If the minimum M_{env} hypothesis is removed, a larger mass loss would be allowed for some stars and the synthetic HB would contain hotter stars. However, the absence of such hot HB stars in Galactic globular clusters in general supports the minimum M_{env} hypothesis[5]. Table 5 lists the

[5] While there are several clusters that are known to contain quite hot HB stars (e.g. M 15, NGC 6752, NGC 1904, & ω Cen), only a few of such hot stars are believed to have an M_{env} smaller than 0.01 $M_{\odot}$. If such hot stars with

estimated mass of the RR Lyrae variables M_{RR}, the mass of the RGB stars at the tip M_{RG}, and the best fitting η for the metal-poor stars.

The estimated η depends on the assumed ages of the globular clusters used in this study. We have chosen 12 – 16 Gyr as an acceptable age range of the Galactic globular clusters M15 and M3 following Chaboyer, Demarque, & Sarajedini (1996). The line with asterisks in the top panels of Figure 3 is the locus of the mass loss in the adopted age range, and this yields the estimated mass loss efficiency of $\eta \approx 0.2 - 0.5$, which is in good agreement with the estimates from the previous studies of metal-poor stars as introduced above. Previous studies (see above) seem to suggest that estimated η's for metal-poor stars are more consistent with one another than for metal-rich stars, in which η varies from 0.25 to 2 – 3. Despite the large uncertainty, this seems to suggest a metallicity-dependence of η in the sense of increasing η with increasing metallicity if, as suggested by Reimers (1975), $\eta \approx 1$ for $Z = Z_{\odot}$.

Figure 4 shows the mass loss estimates, ΔM , for metal-rich stars. There are two general trends to be noted in Figures 3 – 4. Firstly, ΔM generally increases as age increases mainly because M_{RG} decreases with increasing age and the lifetime of a red giant (t_H) becomes significantly longer as its mass (M_{RG}) decreases. Secondly, ΔM reaches a maximum when M_{RG} becomes fairly low. This is because, below this mass, the stellar evolutionary pace is slower than the stellar core growing pace. The mass loss is a product of the two competing time scales, the evolutionary time scale on the RGB and the core growth time scale. Figure 5 shows that ΔM increases as M_{RG} decreases until a certain mass ($M_{RG} \approx 1\ M_{\odot}$ in case of $Z = Z_{\odot}$) is reached because t_H increases as M_{RG} decreases and ΔM obviously increases as t_H increases. Below this mass, however, the evolutionary pace is much slower than the core growing pace, so before the star reaches the tip of the RGB, its core becomes large enough to cause $M_{env} \leq 0.01\ M_{\odot}$. Thus a further evolution on the RGB is halted and the post-RGB phase begins. The post-RGB stars with Menv $< 0.01\ M_{\odot}$ are assumed not to become HB stars but to become WD stars following the $M = 0.453\ M_{\odot}$ track of Sweigart et al. (1974). As discussed above, it is possible that some red giant stars with total masses very nearly equal to the helium ignition core mass will start core helium burning while or after crossing from red to blue giant in the HR-diagram (Demarque & Mengel 1971; Castellani & Castellani 1993; D'Cruz et al. 1996). In this crucial mass range, the mass loss estimation is highly sensitive to how the mass loss takes place (which is poorly known), and thus it has to be carried out with much caution. The same phenomenon exists even if the minimum M_{env} hypothesis is removed.

One can avoid such complications by including mass loss in the stellar evolution calculations from the beginning, if the mass loss mechanism were better understood. However, the current

---

$M_{env} < 0.01\ M_{\odot}$ are remnants of the single stellar evolution, they may provide counterexamples to the minimum M_{env} hypothesis. However, very low mass envelope HB stars might instead be created by mass transfer in binary systems (Mengel, Norris & Gross 1976), or by close interactions in dense parts of globular clusters (Bailyn 1995; Fusi Pecci et al. 1993). In this paper we have considered only the evolution of single, non-interacting stars.

standard models do not yet take into account mass loss simply because the understanding about mass loss is still primitive. Reimers' formula suggests most mass loss takes place near the end of the RGB where surface gravity becomes smallest. Moreover, theoretical hydrodynamical models (Bowen & Willson 1991; Willson, Bowen, & Struck 1996) suggest that mass loss on the RGB is an even more abrupt phenomenon near the end of the RGB than predicted by Reimers' formula. Willson (1996, private communication) even suggested that it would be closer to truth to remove a certain mass from the star at the tip of the RGB than to include Reimers' formula in the stellar evolutionary calculations. If this is true, whether a mass loss formula is included in the construction of the tracks or not causes little difference on the stellar evolution and on the estimated mass loss. It may even be prudent not to include an arbitrary mass loss formula in the evolutionary calculations untill a more reliable mass loss formula becomes available.

The theoretical hydrodynamical models suggest that mass loss takes place when the star reaches a certain critical luminosity (the "cliff"), which is a function of mass and metallicity. Below the cliff, the mass loss rate is too low to be observable; and above the cliff mass loss takes place so rapidly that the star is unlikely to be observed in this phase of evolution. It is significant that their models precisely reproduce Reimers's formula with $\eta = 1$ for $Z = Z_{\odot}$. Moreover, they explain the positive metallicity-dependence of η which observations may be indicating. While their models have not yet been parameterized for population synthesis, Willson et al. (1996, private communication) advise using Reimers' formula with variable η in the sense that η increases as metallicity increases. We call this *the variable η hypothesis*. Table 6 shows the suggested η for different metallicity.

The population synthesis models in this study have all been constructed using values of $\eta =$ 0.3, 0.5, 0.7, and 1.0 that roughly span the range of empirical and hydrodynamical estimates. This will allow us to investigate the effects of mass loss efficiency on the model CMDs and SEDs. The impact of the variable η hypothesis, which has been investigated earlier (Greggio & Renzini 1990) for single abundance models, will be revisited for the composite galaxy models in our next paper (Yi, Demarque, & Oemler 1997).

3.3. Core helium-burning phase: post-RGB

We adopt the evolutionary tracks of core helium-burning phase mainly from YDK. Since YDK do not provide post-AGB (PAGB) tracks, the PAGB tracks of Kiel group (Schönberner 1979; Schönberner 1983; Blöcker & Schönberner 1990) have been adopted. The YDK HB tracks in this study are the short version (plus symbols in Figures 1 – 2 of YDK) of the full tracks (as solid lines in their Figures 1 – 2). The time step on each HB track is 5 Myr and the mass step is approximately 0.04 $M_{\odot}$, with smaller steps near the blue end of the HB as listed in Table 1 of YDK. The masses of the PAGB stars and WD's and the process that determines them are yet to be understood. Meanwhile, Kiel group's models of $M = 0.546$, 0.565, and 0.598 $M_{\odot}$ have been used in the actual population synthesis. One of these three models was chosen as the progeny

of an HB star (almost arbitrarily) depending on the mass of the HB star; that is, 0.546, 0.565, and 0.598 $M_{\odot}$ models were chosen for the HB stars with $M \leq 0.56$, $M = 0.60$, and $M \geq 0.64$. However, the choice of the model does not affect the resulting model integrated spectrum much because PAGB stars are not likely to be the major UV sources when a galaxy shows a strong UV upturn, as will be shown in Section 4.1.

YDK (Figures 1 – 2 of YDK) show that late stellar evolution in the core helium-burning phase, especially in metal-rich galaxies, is very complicated. And, such evolved, metal-rich core helium-burning stars are potentially significant UV sources. Therefore, in order to fully incorporate the complete evolution of core helium-burning stars in the population synthesis code, a physically plausible treatment of the phase is crucial.

The modified gaussian mass distribution (Lee et al. 1990), first invented by Rood (1973) and later modified and elaborated on by Lee et al., has been assumed in this study for the core helium-burning phase as follows:

$$\Psi(M) \, = \, \Psi_0 \, [\, M \, - \, (\overline{M_{HB}} \, - \, \Delta M) \,] \, (M_{RG} \, - \, M) \; exp \, [\, - \, \frac{(\overline{M_{HB}} \, - \, M)^2}{\sigma^2} \,] \tag{7}$$

where σ ($\equiv 2\sigma_{sd}$) is a mass dispersion factor, Ψ_0 is a normalization factor, and $\overline{M_{HB}}$ ($\equiv M_{RG} - \Delta M$) is the mean mass of HB stars. Three values of σ (0.01, 0.06, and 0.99 in $M_{\odot}$) have been chosen to represent distributions similar to a delta-function, a globular-cluster-function (Lee et al. 1990), and a near-constant-function, respectively. While the true value of σ is still quite uncertain (Rood 1973; Smith & Norris 1983; Lee et al. 1990; Walker 1992; Catelan 1993), we have chosen σ = 0.06 $M_{\odot}$ as the "standard" value in this study following empirical (but, with no physical basis) choices of Rood (1973) and Lee et al. (1990). The shape of the functions are shown in Figure 6. In actual calculations, we first estimate the mass loss as a function of age and metallicity, then, apply the gaussian distribution on the mass loss[6]. Assumption of a (modified) gaussian function for the HB mass distribution has been questioned (Smith & Norris 1983; Rood 1990; Ferraro et al. 1992; Dixon et al. 1996). However, the single-gaussian distribution has been very successful in reproducing the observed HB morphology in Galactic globular clusters (Lee et al. 1990; Lee et al. 1994; Dixon et al. 1996; Catelan 1993).

The total number of core helium-burning stars, N_{He}, is as follows:

$$N_{He} \, = \, \overline{t_{He}} \, R_{He} \tag{8}$$

where $\overline{t_{He}}$ is the lifetime of the core helium-burning star of $M = \overline{M_{HB}}$, and R_{He} is the rate at which stars leave the RGB for the core helium-burning stage. So, at a fixed time, there will be

[6] Recently, Jørgensen & Thejll (1993a) and D'Cruz et al. (1996) attempted to explain the width of the HB of Galactic globular clusters by means of a spread in η (mass loss efficiency) rather than a spread in mass loss. Jørgensen & Thejll (1993a) noted that "star-to-star variations of η, between $\eta = 0.0$ and $\eta = 0.7$ can explain the HB morphology in typical globular clusters". It would be very interesting to investigate the effect of such HB treatments to the UV population synthesis.

N_{He} core helium-burning stars on all post-RGB phases. The rate, R_{He} in number of stars per unit time interval $t_1 - t_2$ is defined to be

$$R_{He} = \frac{\alpha}{t_1 - t_2} \int_{M_{GB}(t_2)}^{M_{GB}(t_1)} M^{-(x+1)}\, dM. \tag{9}$$

The calculated probability, $\Psi(M)$, is applied to each evolutionary track according to its mass M_i. There is a different list of stars for different chemical compositions, and each track has a number of evolutionary points with evolutionary time scale information[7]. Thus, the number of stars at the jth evolutionary point on the ith track will be

$$n_{i,j} = \Psi(M_i)\, N_{He}\, \frac{t_{i,j}}{t_i} \tag{10}$$

and

$$t_i = \sum_j t_{i,j} \tag{11}$$

where $\Psi(M_i)$ is the probability of the star of $M = M_i$ to be present, $t_{i,j}$ is the time spent by the ith star in the table near the jth position in the CMD and t_i is the lifetime of the ith star in the post-RGB phase. The sum of the probability $\Psi(M_i)$ should be unity:

$$\Psi = \sum_i \Psi(M_i) = 1. \tag{12}$$

Then the total flux from the core helium-burning stars, F_λ^{He}, is

$$F_\lambda^{He} = \sum_i \sum_j f_{\lambda,i,j}\, n_{i,j}, \tag{13}$$

where $f_{\lambda,i,j}$ is the flux from the ith star in the list of post-RGB stars near the jth evolutionary point.

4. Effects of input parameters

Spectral evolution of galaxies in the UV is much more uncertain than that in the optical band because it is more sensitive to the evolution of post-RGB stars which are less well understood than the MS – RGB stars that dominate the optical flux. It is important to understand first the effects of input parameters on the resulting CMD and UV SED in order to answer the questions related to the spectral evolution of the galaxy, including the UV upturn phenomenon.

Primary parameters affecting the UV flux are age and metallicity. These are the most fundamental quantities in describing stellar populations, because they predominantly determine

[7]Evolutionary time scale: how long a star stays within a box of given size in the CMD.

the $T_{\rm eff}$'s of post-RGB stars. We would like to investigate whether metal-rich old stellar systems, such as giant elliptical galaxies, are capable of exhibiting a pronounced UV flux. Secondary parameters include mass loss efficiency, galactic helium enrichment parameter, form of the dispersion in mass loss, and the slope of IMF, while these parameters are not necessarily less important in producing UV flux than the primary parameters. We assume in this study that all stars in a model stellar system form in an instantaneous starburst.

4.1. Age and metallicity: primary parameters

The effects of age and metallicity in old stellar systems have recently been widely recognized through studies of Greggio & Renzini (1990), Bressan et al. (1994), and of Dorman et al. (1995). In this section, we would like to provide a simple explanation of the basic conclusions of such previous studies by means of stellar evolution theory. We also illustrate that core helium-burning stars are a more likely major UV source in old stellar systems than PAGB stars. Both a higher age and a higher metallicity cause a galaxy to look redder in the optical band mainly because MS and RGB stars become cooler as they age and as metallicity increases, as is clearly shown in Figures 7 – 12. The effects of age and metallicity on the UV flux are more complicated, particularly because the major UV sources vary with time. Before we discuss the details, it is important to remember that we are investigating the effects of age and metallicity while other parameters, such as η, are kept constant. If other parameters are age-dependent and/or metallicity-dependent the true effects of age and metallicity become much more complicated.

4.1.1. Age

The major UV sources vary with time. As seen in Figures 7 – 12, PAGB stars are the only far-UV sources in the early ($\lesssim$ 5 – 10 Gyr, depending on the metallicity) history of galaxy evolution, when the majority of core helium-burning stars are still too cool to produce any UV light. However, once the galaxy is old enough to develop a substantial number of hot core helium-burning stars, those stars dominate the UV spectrum.

In order to investigate the light contribution from various sources, we first arbitrarily divide the core helium-burning stage into two: central helium-burning stage and shell helium-burning stage[8]. The central helium-burning stage is defined as the stage where most of the helium-burning takes place near the center of the star. This stage lasts from the zero age HB (ZAHB) to the point where the central helium is almost exhausted ($Y_c = 0.01$). Similarly, the shell helium-burning stage is defined as the stage that stretches from this point until the star reaches either the tip of

[8]The terms, "core helium-burning" and "central helium-burning", may be confusing. Readers should pay attention to the different definitions of the terms.

the AGB or the beginning of the WD phase, whichever comes first. So the central helium-burning stage is generally referred to as the HB, and the shell helium-burning stage as the post-HB phase including the evolved HB, the AGB and the slow blue phase (SBP). These two stages are denoted as crosses and squares in Figure 13.

Assuming that all the stars in elliptical galaxies have formed in an instantaneous burst, Figure 14 shows that central and shell helium-burning stars are far more efficient UV sources than PAGB stars in old galaxies. The upper and lower panels of Figure 14 show the light contribution from various evolutionary stages in young and old *metal-rich* model galaxies. It shows that MS and RGB stars are the dominant sources in the visible range at all times. The far-UV spectrum is, however, mainly dominated by highly evolved stars. At small ages, PAGB and MS Turn-Off stars are the dominant far-UV and near-UV sources (the upper panel), respectively. However, such galaxies do not exhibit any significant amount of UV flux, as shown in the 5 Gyr old models in Figures 10 – 12. The critical moment which divides the periods in which PAGB stars or core helium-burning stars dominate the far-UV flux is a sensitive function of chemical composition and other parameters (such as η). In the case of the extreme-UV ($\lambda \lesssim 300$Å), PAGB stars always dominate because of their high $T_{\rm eff}$'s. However, once galaxies become old enough to contain hot HB stars, shell helium-burning stars dominate the flux in the far-UV ($\lambda \approx 300$ – 1,500 Å), while both central and shell helium-burning stars are equally important in the near-UV ($\lambda \approx$ 1,500 – 3,000 Å).

The effect of age on the UV flux is relatively simple. Figures 15 – 16 show the UV-to-V colors as a function of age and metallicity. The model magnitudes are defined as $m_\lambda = -2.5 \log < f_\lambda >$ where $< f_\lambda >$ is the mean flux in the bandpass. The $< f(1500) >$, $< f(2500) >$, and $< f(V) >$ are defined by averaging the flux within the ranges 1250 – 1850 Å, 2200 – 2800 Å(Dorman et al. 1995), and 5055 – 5945 Å(Allen 1976), respectively. The observational data are from Table 1 – 2 of Dorman et al. (1995). From their table, we selected the clusters for which both m(1500)-V and m(2500)-V are available. They are mostly *ANS* or *OAO*-2 data. The UIT data of NGC 1904 (M 79) and NGC 5139 (ω Cen) have also been adapted. As a result, three clusters (NGC 1904, NGC 5139, and NGC 5272) have two data points in our adapted cluster sample. We excluded the IUE data because the IUE aperture is so small that IUE data do not represent the integrated light properly (Dorman et al. 1995). In case of metal-poor systems (Figure 15), UV-to-V colors become redder with age for a while as the MS Turn-Off stars, the major UV sources in young metal-poor systems, become redder with time, and then they turn around to become bluer as HB stars get hotter. Most metal-poor globular clusters are reasonably matched by the models with $\eta = 0.5$ but metal-rich globular clusters like NGC 6388 and 47 Tuc are not matched by the same models[9]. This issue of η will be discussed in the next section. Similarly, metal-rich elliptical galaxies are reasonably reproduced by the models with $\eta = 0.7$ in Figure 16.

[9]The m(1500)-V of 47 Tuc obtained by *OAO*-2 is likely to be the lower (bluest) limit because there is one bright PAGB star in *OAO*-2's large aperture (Dorman et al. 1995).

4.1.2. Metallicity

The contribution from each evolutionary stage to the UV flux also varies with metallicity because the post-HB evolutionary pattern differs according to metallicity, as shown in Figures 1 – 2 of YDK. Since the UV-bright SBP phenomenon becomes far more prominent in more metal-rich stars, the contribution from the shell helium-burning stars in the far-UV is more conspicuous in metal-rich models (Figure 17).

It should be noted that the light contribution from evolved core helium-burning stars to the total U band flux ($\lambda \approx$ 3,000 - 4,000 Å) is not negligible. The lower panels of Figures 14 and 17 suggest that substantial amount of the total light comes from such evolved stars. However, note that the precise quantity highly depends on the adopted input parameters. Earlier population synthesis studies (e.g. Tinsley 1972; O'Connell 1976) noticed that population synthesis models, that did not include such evolved stars in an adequate way, were predicting much redder $U - B$ colors than observed. They suggested that this mismatch could originate from the presence of young stars in giant elliptical galaxies. However, Gunn, Stryker, & Tinsley (1981) recognized the lack of empirical support for the young star interpretation, and suggested blue stragglers and what we now call PAGB stars as possible candidates for the observed UV flux. We understand now, as clearly shown in Figures 14 and 17, that a proper treatment of evolved stars, especially with a realistic mass dispersion on the HB, enhances the UV – U band flux significantly, as pointed out by Burstein et al. (1988) earlier[10]. This short wavelength region is extremely sensitive not only to age and metallicity of the galaxy but also to various input parameters, including mass loss efficiency and the HB mass distribution, as will be shown in the following sections.

The overall effect of metallicity is more complicated than that of age because it is a product of several competing effects. Even when we consider only the period in which the core helium-burning stars are the main UV sources, it is better to see the metallicity effect in two different metallicity domains, (1) $Z < Z_{\odot}$ and (2) $Z \gtrsim Z_{\odot}$,

When $Z < Z_{\odot}$, UV-to-V flux ratios decrease with increasing metallicity. This is a result of the following competing effects. (1) The temperature of the HB stars decreases dramatically as metallicity increases, (2) more metal-rich stars stay on the MS – RGB longer (Greggio & Renzini 1990; Jørgensen & Thejll 1993b), but (3) a larger mass loss of more metal-rich stars for a fixed η (Figures 3 – 4) compensates for these two effects (Jørgensen & Thejll 1993b). The phenomenon (2) is mainly caused by the delay of the evolution due to the opacity effect. Consequently, the phenomenon (2) makes a more metal-rich cluster have more massive red giants at a fixed age, but (3) compensates for this effect and makes the $\overline{M_{HB}}$ of more metal-rich clusters smaller than that of metal-poor clsuters in this metallicity domain. However, the phenomenon in (1) again negates the result of the competition between that of (2) and (3). The net effect of all these

[10]The referee pointed out that the "excess" near-UV (U band) light in elliptical galaxies could also be due to intermediate temperature (younger) main sequence stars.

competitions is a decrease in the UV-to-V flux ratios with increasing metallicity which is consistent with observations, as illustrated in Figure 15. In Figure 15, three metal-poor models covering 1 – 25 Gyr of age are compared with globular cluster data. It is clear that both observations and models indicate that more metal-rich systems in this metal-poor regime are redder in these UV-to-V colors. It should be noted that this trend (the correlation between the UV-to-V ratios and metallicity) is based on the assumption that other parameters are identical. In the case of Galactic globular clusters, it has been suggested that there is a substantial spread in age among them which influences the HB morphology and thus the flux ratios. A large scatter in the flux ratios in Figure 16 may have been caused by such differences in cluster parameters.

In the metal-rich regime $Z \gtrsim Z_{\odot}$, the evolutionary phenomena are quite different. Firstly, the higher the metallicity, the faster the MS – RGB evolution, because the luminosity from the hydrogen burning is significantly sensitive to the mean molecular weight that is determined by the chemical composition. This has been noticed previously by a number of workers (e.g. Greggio & Renzini 1990; Jørgensen & Thejll 1993b). Under the assumption of a positive $\Delta Y/\Delta Z$ ($\approx 2 - 3$ in this study), a higher metallicity means a higher helium abundance. A higher helium abundance causes a higher mean molecular weight that results in a faster stellar evolution (see YDK). This causes the M_{RG} of more metal-rich stars at a fixed age to be smaller. Secondly, the increase in mass loss as a function of metallicity (Figures 3 – 4) makes $\overline{M_{HB}}$ of more metal-rich HB stars much smaller at a fixed age. In addition to this, even many of the metal-rich HB stars that are born as extremely cool stars quickly evolve to become UV-bright stars (namely, SBP stars in Figures 1 – 2 of YDK). As a result, more metal-rich galaxies are expected to contain more UV-bright stars at a given age in this metal-rich regime, given other parameters fixed. This is illustrated in Figure 16: the more metal-rich, the bluer. Figure 16 seems to suggest that the galaxy data are better fitted by the $Z = 0.01$ model than more metal-rich models. We believe that this is an artifact that is produced by the comparison between the galaxy data and single-abundance models. Obviously, galaxies are not composed of stars of a single abundance only. The effect of the composite population treatment will be discussed in detail in our next paper.

The data and models in Figure 18 show that metal-poor globular clusters in general exhibit bluer m(1500)-V and m(2500)-V colors than elliptical galaxies (bottom panel of Figure 18). This is mainly because of the opacity effect on the HB stars (in the case of m(1500)-V) and on the MS stars (in the case of m(2500)-V). For a given age, the opacity effect on the stellar evolution causes metal-poor blue HB stars to have higher $T_{\rm eff}$'s than metal-rich counterparts, even though the mean mass of metal-rich HB stars, $\overline{M_{HB}}$, are likely to be smaller (note that, given the other parameters fixed, a lower-mass HB star is hotter) according to Reimers' formula (see Figures 3 – 4 and Table 1 –4). Moreover, even if their $T_{\rm eff}$'s are identical, the opacity effect (via the line-blanketing effect in the spectral synthesis) causes more metal-rich HB stars to look much redder than metal-poor HB stars. For the same reason, metal-poor systems show bluer m(2500)-V colors, but this time because of the opacity effect on *MS stars* (Dorman et al. 1995). As a result, metal-poor populations exhibit stronger UV-to-V flux ratios than metal-rich populations.

However, metal-poor populations with such blue UV-to-V colors do not exhibit a "UV upturn" (the continuously increasing flux with decreasing wavelength below 2,500 Å). Instead, their UV spectra, even for the UV-strong globular clusters, are rather flat below 2,500 Å. Consequently, globular clusters have redder m(1500)-m(2500) colors than elliptical galaxies, as shown in the top panel of Figure 18. So, it should be said that only elliptical galaxies exhibit a "UV upturn" in a strict sense, as models predict in Figure 18. This result disagrees with Park & Lee (1997)'s recent suggestion. Details will be discussed in our next paper.

4.2. Mass loss efficiency

Figures 19 – 20 show that the magnitude of the UV flux is sensitive to the mass loss efficiency η in Reimers' formula. A larger η results in lower-mass, hotter HB stars. Therefore, a value for mass loss efficiency should be adopted carefully and with sufficient justification. The probable range of η seems to be 0.3 – 1.0 (or even 2) with a possible positive metallicity-dependence supported both by observations and hydrodynamical models, as discussed in Section 3.2. Such sensitivity of the UV flux to the mass loss efficiency has significant implications.

If Reimers' formula is an adequate approximation of reality, η of stars of $Z \gtrsim Z_{\odot}$ should be near or larger than 0.7 (this value depends on the assumed metallicity of giant elliptical galaxies) in order for a metal-rich elliptical galaxy to exhibit a UV upturn within a Hubble time[11]. Old, metal-rich galaxies should have an appreciable number of UV-bright stars and a noticeable UV upturn as long as $\eta \gtrsim 0.7$ for metal-rich ($Z \gtrsim Z_{\odot}$) stars. On the other hand, if $\eta \lesssim 0.7$ for metal-poor stars, as both observations and theory suggest, metal-poor stars *cannot* be major UV sources in elliptical galaxies because they do not produce sufficient far-UV flux (e.g. m(1500)-m(2500) color) within a Hubble time, as Figure 20 shows. This problem becomes worse when even shorter wavelength regions ($\lesssim$ 1,500 Å) are compared, because the UV spectral energy distributions of giant elliptical galaxies have much higher far-UV flux than near-UV flux, and this cannot be produced by metal-poor models unless η is unrealistically high. Even if larger η-models (e.g. 1.0) may reproduce such high far-UV flux (bottom panel in Figure 20), the predicted overal spectral shape in the UV does not look similar to what is observed. Detailed quantitative study will be shortly presented by Yi et al. (1997).

Conversely, the magnitude of the UV upturn can be used to set a constraint on the mass loss efficiency of Galactic globular clusters whose age and metallicity are independently estimated[12]. For instance, if we compare the far-UV spectrum of M 79 (Figure 5 in Dixon et al. 1996) with

[11]We assume that a Hubble time is slightly larger than the age of the oldest Galactic globular cluster estimated using the same stellar evolutionary calculations as the ones used in this study. This study is based on the stellar models that suggest an age of approximately 15 Gyr for the oldest Galactic globular clusters (Chaboyer et al. 1996).

[12]In order for this method to be reliable, far-UV ($\lesssim$ 1,500 Å) spectra should be available.

Figure 20, the model with $\eta \approx 0.5$ reproduces the empirical spectrum best, assuming 15 Gyr for its age and "standard" values of model parameters ($x = 1.35$, $\sigma = 0.06$).

Figure 21 illustrates the η-dependence of metal-poor models. As discussed earlier in Section 3.2, low-η models ($\eta = 0.3$ – 0.5) reasonably match the observations at an age of $\approx$ 15 Gyrs. However, the metal-rich clusters (filled squares, e.g. NGC 6388) cannot be matched by the models with consistent ages. For example, if $\eta = 0.3$ even for such metal-rich globular clusters, UV color fitting would suggest NGC 6388 is almost 25 Gyrs old, which is much higher than the average isochrone-age of globular clusters ($\approx$ 15 Gyr, Chaboyer et al. 1996). If a larger η is adopted for such metal-rich globular clusters instead, their colors can be reproduced successfully at a reasonable age. For instance, the age estimate for NGC 6388 would be $\approx$ 19 Gyr and 15 Gyr if $\eta = 0.5$ and 0.7, respectively. If other complexities are ignored at the moment, this suggests $\eta \approx 0.7$ for $Z \approx 0.006$ (the metallicity of NGC 6388), which is higher than the best fitting η for metal-poor clusters. This metallicity-dependence of η is consistent with the variable-η hypothesis discussed in Section 3.2. Elliptical galaxies are also better matched by high-η models ($\eta \gtrsim 0.7$), as shown in Figure 22, which is again consistent with the variable-η hypothesis. Note that in this diagram we use m(1500)-m(2500) as the y-axis because m(1500)-m(2500) describes the UV upturn strength of galaxies better. Regardless of metallicity, η certainly plays a very important role in model UV flux in the sense that a higher-η, at least in the rage $\eta = 0.3$ – 1.0, leads to a higher UV flux.

4.3. $\Delta Y/\Delta Z$

The galactic helium enrichment parameter, $\Delta Y/\Delta Z$, is another important determinant of the UV flux, not only because it affects the pace of evolution of MS and RGB stars (Greggio & Renzini 1990; Jørgensen & Thejll 1993b), but also because metal-rich stars with a higher $\Delta Y/\Delta Z$ become UV-bright more readily (Horch et al. 1992; Dorman et al. 1993; YDK). This phenomenon is more significant when $Z \gtrsim Z_{\odot}$, with an implicit assumption of a positive $\Delta Y/\Delta Z$. Therefore, a metal-rich galaxy with a higher value of $\Delta Y/\Delta Z$ produces a higher UV flux, as shown in Figures 23 – 24. Qualitatively, models with $\Delta Y/\Delta Z = 2$ develop a similar magnitude of UV flux to that of $\Delta Y/\Delta Z = 3$ at approximately 10 – 20 % greater ages. Despite such a difference, it is difficult to estimate the true $\Delta Y/\Delta Z$ from UV magnitudes only because the evolutionary paths for different $\Delta Y/\Delta Z$ are very similar as shown in Figure 24, unless their ages are already known.

If $\Delta Y/\Delta Z$ is not positive (a very unrealistic assumption in the light of what is known about nucleosynthesis in massive stars, see e.g. Maeder 1991), in other words, if helium does not increase with increasing metallicity, several complicated effects will compete with one another: (1) The SBP (slow blue phase) phenomenon will not be significant even in metal-rich (but, not unrealistically metal-rich) populations (Dorman et al. 1993; Bressan et al. 1994). This reduces the UV flux from such hot SBP stars. (2) The evolutionary pace of the more metal-rich stars will perhaps become slower because the opacity effect will overwhelm the hydrogen luminosity-mean molecular weight

effect (See Eqn. 3 in YDK). This is similar to the metallicity effect on the evolutionary pace of subsolar-abundance stars; namely, the more metal-rich, the slower the evolutionary pace on the MS and RGB if $Z \lesssim Z_{\odot}$. This causes a cooler HB. (3) But, the mass loss will still increase with metallicity regardless of helium abundance. This will cause HB stars to become hotter. The final result of this competition is not trivial to guess. Unfortunately, the stellar models of $\Delta Y/\Delta Z = 0$ are not yet available for numerical experiments.

4.4. IMF

The slope of IMF, x, as defined in Eqn. 3, has a very small effect on the resulting UV flux as shown in Figures 25 – 27, even if x differs from one galaxy to another significantly. A model with a smaller x sends more stars from the MS both to the RGB and to the HB and results in an increase in flux in all wavelength regions. So the relative flux is not much affected. Many observations have supported $x \approx 1.35$ (Salpeter 1955; Miller & Scalo 1979; Larson 1992; Larson 1995), and thus we have little justification for adopting a significantly different value. The effect of the difference in various forms of IMF for the very low-mass stars on the resulting SEDs is negligible because they contribute little to the total light of the host galaxy although they could affect the calculated mass-to-luminosity ratio significantly.

4.5. Mass dispersion on the HB

A smooth mass dispersion on the HB has not been seriously taken into account as an input parameter in earlier population synthesis studies[13], although it is very important to the resulting SED in the UV. Its effect is not monotonic. When a galaxy is young, and has mostly red HB stars, allowing a larger dispersion in mass leads to a larger number of hot HB stars, which results in a stronger UV flux (Figure 27). On the other hand, when a galaxy is already old enough to have most of its HB stars on the hot side, a larger mass dispersion causes a weaker UV flux (Figure 28). These effects on the colors are illustrated in Figure 29. As is the case of $\Delta Y/\Delta Z$, it is difficult to choose an optimal σ from the UV colors because models with even very different values of σ follow very similar evolutionary paths (Figure 29) unless the age of the galaxies is known a priori.

[13] Dorman et al. (1995) treated the HB as a product of two different values of mass loss on the RGB (i.e. bimodal distribution in the mass loss: two peaks - a red HB clump and a blue HB clump - instead of a smooth distribution) to understand how large a fraction of hot HB components is needed to account for the observed UV flux of elliptical galaxies. Their blue HB clump is either by δ-function or by constant-function within a certain mass range, both of which are arbitrary. Although this is a much improved effort compared to previous works in terms of the HB treatment, it is still ad hoc because such bimodality is supported (at least so far) only by a few globular clusters, e.g. NGC 2808 (Crocker, Rood, & O'Connell 1988). A single-gaussian mass distribution reproduces the HB distribution adequately (Lee et al. 1990; Lee et al. 1994), as discussed in Section 3.2.

Because of this complex sensitivity of the UV flux to the assumed HB mass distribution, a realistic HB treatment is essential to the UV population synthesis. Oversimplified HB treatments, such as a clump star assumption[14], a single-mass assumption[15] and a flat distribution[16], are inadequate for UV studies unless there is a sufficient justification.

5. Summary

Recently, several groups have been using the evolutionary population synthesis (EPS) technique in the hope of understanding the stellar content and the evolution of giant elliptical galaxies. Most of these studies are aimed at solving the so-called UV upturn mystery. Although EPS in the UV is a powerful technique for these purposes, its dependence on various input parameters has not been widely known. Therefore, both modelers and model users are vulnerable to misinterpretations of the results from their population synthesis studies.

The EPS technique has been described in this study in detail. We show that the model UV flux is very sensitive to several input parameters as various earlier studies pointed out. These input parameters include not only age and metallicity, but also mass loss efficiency η, galactic helium enrichment parameter $\Delta Y/\Delta Z$, and mass distribution on the HB. The effects of these parameters are as follows.

1. Once MS turn-off stars become too cool to dominate the near-UV integrated flux, the relative strength of UV flux to visible flux always increases with age because a larger number of hotter core helium-burning stars develop as a galaxy ages. Before this point, UV-to-V colors become redder with increasing age as MS stars, the major near-UV sources at low ages, become cooler. This turning point is sensitive to metallicity and other parameters. It could be approximately 1 Gyr or even smaller if $Z \gtrsim 0.06$ but could be as large as 10 Gyrs if $Z = 0.0004$. A possibility that giant elliptical galaxies have a substantial fraction of very young (< 1 Gyr) stars is ignored in this study because of lack of empirical support (O'Connell et al. 1992; Bertola et al. 1993).

2. In the metal-rich regime ($Z \gtrsim Z_{\odot}$), metallicity has a positive impact on the UV flux once a model galaxy is old enough to have a substantial number of hot core helium-burning stars. This is caused mainly by the following phenomena in stellar evolution: under the assumption of a moderate $\Delta Y/\Delta Z\,(\approx 2 - 3)$, (1) more metal-rich stars evolve faster when $Z \gtrsim Z_{\odot}$, which results in a quicker hot HB development, (2) more metal-rich red giants experience a larger mass loss, and (3) more metal-rich core helium-burning stars become UV-bright stars in the slow blue

[14]It assumes that all the HB stars have the same physical properties, luminosities and temperature, ignoring the mass dispersion on the HB and the advanced evolution beyond the ZAHB.

[15]It assumes that all the HB stars have the same mass and follow the same evolution.

[16]This assumption allows a mass dispersion but does not consider any concentration of stars at some mass.

phase (SBP) more easily. This result is in agreement with Brown et al. (1997)'s recent spectral analysis which suggests that "models with supersolar metal abundance and helium best reproduce the flux across the entire HUT wavelength range...". Optical spectra of giant elliptical galaxies suggest $Z \gtrsim Z_{\odot}$. In the metal-poor regime, the metallicity effect is reversed, however. This is mainly because the opacity effect overwhelms the metallicity-mass loss relation. In addition, in this metal-poor regime, an increase in metallicity causes stars on the MS – RGB to evolve more slowly and causes the HB to look redder.

3. Because the UV-bright phase (the SBP) of core helium-burning stars is positively correlated with helium abundance, a model galaxy with a higher $\Delta Y/\Delta Z$ exhibits a stronger UV upturn. This agrees with the result of Greggio & Renzini (1990). If, as we expect, the true $\Delta Y/\Delta Z$ is within the range 2 – 3, then the degree of the sensitivity seems moderate. The effect of $\Delta Y/\Delta Z$ and the cause of the effect are similar to those of metallicity described above. A model with $\Delta Y/\Delta Z = 2$ would develop a UV flux with a similar magnitude to that of a model with $\Delta Y/\Delta Z = 3$ at slightly later time (approximately 10 – 20 % of their ages).

4. A larger mass loss efficiency, η, causes a stronger UV upturn because it causes a hotter HB. The probable range of η is 0.3 – 1 (or higher) with a large uncertainty and probably with a positive metallicity-dependence suggested by hydrodynamic models. If we admit that the other parameters in this study are relatively better known than η, fixing the other parameters allows us to constrain the true value of η. In the metal-poor regime ($Z \lesssim 0.01$), if we assume that Galactic globular clusters are about 15 billion years old, the IMF slope $x \approx 1.35$, and $\sigma \approx 0.06\ M_{\odot}$, the models with $\eta \approx 0.3$ – 0.5 fit metal-poor cluster data better. However, a larger value-models (e.g. $\eta \approx 0.5$ – 0.7) fit relatively metal-rich globular cluster data (such as NGC 6388) substantially better. Similarly, under the same assumptions as the metal-poor case, only high-η (0.7 – 1.0) models fit the elliptical galaxy data.

5. Mass dispersion on the HB is crucial to the UV flux. A larger dispersion causes a stronger (weaker) UV flux when the HB stars with the average mass are red (blue). Because the effect of σ is large, a population synthesis based on a non-realistic synthetic HB is likely to lead us to erroneous conclusions. We chose $\sigma = 0.06\ M_{\odot}$ from globular cluster studies as our "standard" dispersion. However, this value does not have a physical basis and is poorly known for metal-rich systems.

6. Even a significant change in the IMF slope, x, results in only a slight change in the resulting UV flux in comparison to optical flux. A smaller value of x causes a slightly stronger UV flux, because a model galaxy with a smaller x sends more stars from the RGB to the HB at a fixed time. However, there is little justification for an adoption of a much different IMF slope from the standard one, i.e. $x = 1.35$.

6. Conclusion

Based on this sensitivity study, we conclude as follows. Both the positive correlation between metallicity and UV-to-V colors among elliptical galaxies (Burstein et al. 1988) and the negative correlation between metallicity and UV-to-V colors among globular clusters have been explained. Old, metal-rich populations, such as giant elliptical galaxies, naturally develop a UV upturn within a reasonable time scale ($\lesssim$ Hubble time) without the necessity of the presence of young stars. Low-mass, core helium-burning (HB and evolved HB) stars are more likely to be the main UV sources in the old stellar systems than any other types of stars, as suggested before (e.g. Greggio & Renzini 1990; Horch et al. 1992; Ferguson & Davidsen 1993; Bressan et al. 1994; Dorman et al. 1995; Yi et al. 1995; Brown et al. 1997). For this reason, both metal-poor and metal-rich populations can develop a UV upturn if an arbitrarily large age may be assumed.

Metal-poor models, such as globular clusters, are bluer in m(1500)-V and m(2500)-V than metal-rich models like elliptical galaxies as observations suggest, mainly because of the opacity effect. But, their UV spectra are flat and fail to exhibit a strong UV upturn because they lack very hot HB and post-HB stars. It takes too long (> Hubble time) for a metal-poor population to develop a UV upturn of the observed strength if $\eta \lesssim 0.7$ for metal-poor stars as both observations and hydrodynamical models suggest. For this reason, no metal-poor stellar system has been observed to show a strong UV upturn (i.e. the continuous increase in the UV flux with decreasing wavelength below 2,500 Å) no matter how old it is. Even if metal-poor models with a larger η ($\eta \gtrsim 1.0$, an unrealistic assumption) may reproduce the observed UV-to-V colors of giant elliptical galaxies, the overall spectral shape in the UV would not match the observations very well, as will be quantitatively shown in our next paper (Yi et al. 1997b). On the other hand, metal-rich model populations contain a sufficiently large number of UV-bright SBP stars, in addition to hot HB stars, to exhibit a UV upturn of the observed magnitude unless the input parameters assumed in this study are significantly wrong. Based on this argument, metal-poor stars cannot be the main cause of the UV upturn in giant elliptical galaxies that are obviously composite populations, as long as the majority of stars in giant elliptical galaxies are metal-rich.

Two main effects drive a metal-rich population to develop a UV upturn of the observed magnitude earlier than a metal-poor population. Firstly, metal-rich stars experience a larger amount of mass loss on the RGB when Reimers' formula and a fixed η are used. This generates lower-mass HB stars at a fixed time. This is mainly because a higher opacity causes a larger stellar radius. Reimers' mass loss formula (and our intuition as well) suggests that a smaller surface gravity caused by the larger radius results in a larger mass loss. Secondly, even if some HB stars are not hot on the ZAHB, more metal-rich stars evolve to UV-bright stars more easily.

In conclusion, it is important to realize that the presence of the UV upturn in the spectrum of giant elliptical galaxies becomes neither extraordinary nor unexpected when proper treatments of various evolutionary stages are taken into account. It is a very natural consequence of advanced stellar evolution that has not been known in detail until recently. While the presence of the UV

upturn has been qualitatively understood, the detailed characteristics of the observed UV upturn also have to be reproduced in order to confirm the theoretical explanations. All these aspects will be investigated quantitatively in the following paper (Yi et al. 1997b).

We thank Richard Larson, Robert Zinn, Wayne Landsman, and Sally Heap for useful comments. We are grateful to the anonymous referee for constructive criticisms and clarifications on many points. This work was part of the Ph.D. study of S.Y. (Yi 1996) and was supported in part by NASA grants NAGW-3563 (S.Y. and A.O.), NAG5-1486 and NAG5-2469 (P.D.). Part of this work was performed while S.Y. held a National Research Council-(NASA Goddard Space Flight Center) Research Associateship.

Table 1. Mass loss estimates based on Reimers' formula ($\eta = 0.3$).

t(Gyr)							ΔM ($M_\odot$)							
Z	0.0001	0.0004	0.001	0.004	0.01	0.02	0.04	0.06	0.1	0.01	0.02	0.04	0.06	0.1
Y	0.23	0.23	0.23	0.23	0.25	0.27	0.31	0.35	0.43	0.26	0.29	0.35	0.41	0.53
1	0.032	0.039	0.045	0.063	0.057	0.054	0.048	0.038	0.017	0.049	0.049	0.040	0.029	0.014
2	0.039	0.045	0.052	0.069	0.065	0.067	0.066	0.061	0.044	0.065	0.066	0.066	0.068	0.040
3	0.045	0.052	0.058	0.075	0.073	0.079	0.084	0.083	0.063	0.080	0.083	0.092	0.092	0.067
4	0.052	0.058	0.065	0.081	0.081	0.092	0.102	0.104	0.078	0.087	0.091	0.106	0.101	0.086
5	0.058	0.065	0.071	0.087	0.089	0.097	0.113	0.110	0.094	0.094	0.097	0.113	0.111	0.103
6	0.065	0.072	0.078	0.093	0.096	0.101	0.119	0.116	0.109	0.100	0.102	0.120	0.120	0.121
7	0.070	0.077	0.084	0.100	0.103	0.105	0.124	0.122	0.124	0.107	0.108	0.127	0.129	0.138
8	0.072	0.080	0.087	0.106	0.110	0.110	0.130	0.128	0.136	0.113	0.113	0.134	0.138	0.130
9	0.075	0.082	0.090	0.112	0.117	0.114	0.135	0.134	0.140	0.120	0.119	0.141	0.143	0.121
10	0.077	0.085	0.093	0.115	0.124	0.119	0.140	0.140	0.145	0.126	0.124	0.148	0.147	0.112
11	0.079	0.087	0.095	0.118	0.131	0.123	0.146	0.146	0.149	0.129	0.130	0.155	0.152	0.102
12	0.082	0.090	0.098	0.120	0.135	0.128	0.151	0.151	0.154	0.133	0.132	0.158	0.156	0.093
13	0.084	0.092	0.100	0.123	0.138	0.132	0.157	0.157	0.158	0.136	0.135	0.162	0.160	0.083
14	0.086	0.094	0.103	0.125	0.140	0.136	0.162	0.161	0.162	0.139	0.137	0.165	0.164	0.074
15	0.088	0.097	0.105	0.128	0.143	0.138	0.167	0.163	0.166	0.142	0.139	0.168	0.168	0.065
16	0.091	0.099	0.108	0.131	0.146	0.141	0.170	0.166	0.171	0.146	0.142	0.172	0.173	0.056
17	0.093	0.102	0.111	0.133	0.149	0.143	0.173	0.169	0.175	0.149	0.144	0.175	0.177	0.046
18	0.095	0.104	0.113	0.136	0.152	0.146	0.175	0.172	0.175	0.152	0.147	0.178	0.181	0.037
19	0.097	0.107	0.116	0.138	0.155	0.148	0.178	0.175	0.174	0.156	0.149	0.182	0.181	0.027
20	0.100	0.109	0.118	0.141	0.158	0.151	0.181	0.178	0.172	0.159	0.151	0.185	0.171	0.024
21	0.102	0.112	0.121	0.144	0.161	0.153	0.183	0.181	0.171	0.162	0.154	0.188	0.161	0.028
22	0.104	0.114	0.123	0.146	0.164	0.155	0.186	0.183	0.170	0.165	0.156	0.191	0.150	0.033
23	0.106	0.116	0.126	0.149	0.167	0.158	0.189	0.186	0.168	0.160	0.159	0.195	0.140	0.037
24	0.109	0.119	0.128	0.151	0.170	0.160	0.191	0.189	0.167	0.147	0.161	0.198	0.130	0.042
25	0.111	0.121	0.131	0.154	0.173	0.163	0.194	0.192	0.166	0.134	0.163	0.201	0.120	0.046

Table 2. Mass loss estimates based on Reimers' formula ($\eta = 0.5$).

t(Gyr)							ΔM ($M_\odot$)							
Z	0.0001	0.0004	0.001	0.004	0.01	0.02	0.04	0.06	0.1	0.01	0.02	0.04	0.06	0.1
Y	0.23	0.23	0.23	0.23	0.25	0.27	0.31	0.35	0.43	0.26	0.29	0.35	0.41	0.53
1	0.054	0.064	0.075	0.106	0.093	0.090	0.078	0.065	0.029	0.082	0.082	0.065	0.048	0.024
2	0.065	0.075	0.086	0.116	0.108	0.111	0.109	0.102	0.073	0.108	0.110	0.110	0.113	0.068
3	0.076	0.086	0.097	0.126	0.122	0.132	0.140	0.139	0.105	0.133	0.138	0.154	0.154	0.111
4	0.087	0.097	0.108	0.136	0.136	0.153	0.171	0.174	0.131	0.145	0.152	0.177	0.170	0.144
5	0.097	0.108	0.119	0.146	0.149	0.161	0.189	0.183	0.156	0.156	0.161	0.188	0.185	0.172
6	0.108	0.119	0.130	0.156	0.161	0.168	0.198	0.193	0.182	0.167	0.170	0.200	0.200	0.201
7	0.117	0.129	0.140	0.166	0.172	0.176	0.207	0.203	0.207	0.178	0.179	0.212	0.215	0.230
8	0.122	0.133	0.145	0.176	0.184	0.183	0.216	0.213	0.227	0.189	0.189	0.223	0.231	0.218
9	0.126	0.137	0.149	0.186	0.195	0.191	0.225	0.223	0.234	0.200	0.198	0.235	0.239	0.202
10	0.131	0.141	0.153	0.189	0.207	0.198	0.234	0.233	0.242	0.211	0.207	0.246	0.246	0.186
11	0.136	0.145	0.156	0.191	0.219	0.206	0.243	0.242	0.249	0.215	0.216	0.258	0.253	0.171
12	0.140	0.149	0.159	0.193	0.224	0.213	0.252	0.252	0.256	0.219	0.221	0.263	0.260	0.155
13	0.145	0.153	0.162	0.194	0.229	0.221	0.261	0.262	0.263	0.223	0.225	0.268	0.267	0.140
14	0.149	0.157	0.166	0.196	0.234	0.227	0.270	0.267	0.271	0.227	0.229	0.273	0.274	0.124
15	0.154	0.161	0.169	0.197	0.239	0.231	0.278	0.271	0.278	0.231	0.233	0.278	0.281	0.108
16	0.159	0.165	0.172	0.199	0.244	0.235	0.281	0.275	0.285	0.235	0.237	0.283	0.288	0.093
17	0.163	0.169	0.176	0.201	0.249	0.240	0.284	0.279	0.292	0.240	0.241	0.288	0.295	0.077
18	0.168	0.173	0.179	0.202	0.254	0.244	0.287	0.283	0.292	0.244	0.245	0.293	0.302	0.062
19	0.172	0.177	0.182	0.204	0.258	0.248	0.289	0.288	0.288	0.248	0.249	0.298	0.302	0.046
20	0.177	0.181	0.186	0.206	0.263	0.252	0.292	0.292	0.285	0.252	0.253	0.303	0.285	0.039
21	0.182	0.184	0.189	0.207	0.268	0.256	0.295	0.296	0.282	0.256	0.257	0.308	0.268	0.044
22	0.186	0.189	0.192	0.209	0.273	0.260	0.297	0.300	0.279	0.260	0.261	0.313	0.251	0.049
23	0.191	0.192	0.196	0.211	0.278	0.264	0.300	0.305	0.276	0.264	0.265	0.318	0.234	0.054
24	0.196	0.196	0.199	0.212	0.283	0.268	0.303	0.309	0.273	0.268	0.269	0.323	0.217	0.058
25	0.200	0.200	0.202	0.214	0.288	0.272	0.306	0.313	0.269	0.272	0.273	0.328	0.200	0.063

Table 3. Mass loss estimates based on Reimers' formula ($\eta = 0.7$).

t(Gyr)							ΔM ($M_\odot$)							
Z	0.0001	0.0004	0.001	0.004	0.01	0.02	0.04	0.06	0.1	0.01	0.02	0.04	0.06	0.1
Y	0.23	0.23	0.23	0.23	0.25	0.27	0.31	0.35	0.43	0.26	0.29	0.35	0.41	0.53
1	0.077	0.090	0.105	0.149	0.131	0.125	0.110	0.090	0.040	0.115	0.115	0.092	0.067	0.033
2	0.092	0.105	0.120	0.163	0.151	0.155	0.153	0.142	0.103	0.151	0.153	0.154	0.157	0.094
3	0.107	0.121	0.135	0.176	0.170	0.185	0.196	0.193	0.148	0.187	0.192	0.216	0.215	0.156
4	0.122	0.136	0.151	0.191	0.189	0.215	0.239	0.243	0.183	0.203	0.212	0.247	0.237	0.201
5	0.137	0.151	0.166	0.204	0.208	0.226	0.264	0.257	0.218	0.219	0.225	0.263	0.259	0.242
6	0.152	0.167	0.181	0.218	0.224	0.236	0.277	0.271	0.254	0.234	0.238	0.280	0.280	0.282
7	0.163	0.180	0.196	0.232	0.241	0.247	0.290	0.284	0.289	0.249	0.251	0.296	0.302	0.322
8	0.166	0.182	0.199	0.246	0.257	0.257	0.302	0.298	0.315	0.265	0.264	0.312	0.323	0.305
9	0.168	0.184	0.202	0.260	0.273	0.267	0.315	0.312	0.320	0.280	0.277	0.328	0.330	0.283
10	0.171	0.186	0.204	0.263	0.289	0.278	0.328	0.326	0.326	0.295	0.290	0.345	0.333	0.261
11	0.174	0.189	0.206	0.262	0.306	0.288	0.340	0.340	0.331	0.298	0.303	0.361	0.336	0.239
12	0.176	0.191	0.207	0.262	0.309	0.299	0.353	0.354	0.336	0.301	0.306	0.361	0.338	0.217
13	0.179	0.193	0.209	0.261	0.311	0.309	0.365	0.367	0.341	0.303	0.307	0.360	0.341	0.196
14	0.182	0.195	0.211	0.261	0.312	0.316	0.378	0.368	0.346	0.306	0.309	0.360	0.344	0.174
15	0.184	0.197	0.212	0.260	0.314	0.318	0.389	0.368	0.351	0.309	0.310	0.359	0.347	0.152
16	0.187	0.199	0.214	0.260	0.316	0.319	0.387	0.367	0.356	0.312	0.312	0.359	0.350	0.130
17	0.190	0.202	0.215	0.259	0.317	0.320	0.385	0.366	0.361	0.315	0.314	0.358	0.352	0.108
18	0.192	0.204	0.217	0.259	0.319	0.321	0.384	0.366	0.356	0.317	0.315	0.358	0.355	0.086
19	0.195	0.206	0.219	0.258	0.320	0.322	0.382	0.365	0.349	0.320	0.317	0.357	0.352	0.065
20	0.198	0.208	0.220	0.258	0.322	0.323	0.380	0.365	0.342	0.323	0.318	0.357	0.334	0.054
21	0.200	0.210	0.222	0.257	0.324	0.325	0.378	0.364	0.335	0.326	0.320	0.356	0.316	0.059
22	0.203	0.212	0.223	0.257	0.325	0.326	0.377	0.363	0.327	0.329	0.322	0.356	0.298	0.064
23	0.206	0.215	0.225	0.256	0.327	0.327	0.375	0.363	0.320	0.318	0.323	0.355	0.280	0.068
24	0.208	0.217	0.226	0.256	0.328	0.328	0.373	0.362	0.313	0.295	0.325	0.355	0.262	0.073
25	0.211	0.219	0.228	0.255	0.330	0.329	0.371	0.361	0.305	0.272	0.326	0.354	0.244	0.078

Table 4. Mass loss estimates based on Reimers' formula ($\eta = 1.0$).

t(Gyr)							ΔM ($M_\odot$)							
Z	0.0001	0.0004	0.001	0.004	0.01	0.02	0.04	0.06	0.1	0.01	0.02	0.04	0.06	0.1
Y	0.23	0.23	0.23	0.23	0.25	0.27	0.31	0.35	0.43	0.26	0.29	0.35	0.41	0.53
1	0.109	0.129	0.150	0.212	0.188	0.179	0.157	0.130	0.057	0.164	0.164	0.132	0.095	0.047
2	0.131	0.151	0.172	0.232	0.216	0.222	0.219	0.203	0.146	0.216	0.219	0.220	0.225	0.134
3	0.152	0.172	0.194	0.252	0.243	0.265	0.280	0.277	0.211	0.267	0.275	0.309	0.308	0.222
4	0.174	0.194	0.215	0.272	0.271	0.307	0.342	0.347	0.261	0.291	0.303	0.354	0.338	0.271
5	0.196	0.216	0.237	0.292	0.298	0.322	0.376	0.367	0.312	0.313	0.321	0.377	0.369	0.307
6	0.217	0.238	0.259	0.312	0.321	0.337	0.391	0.387	0.362	0.335	0.340	0.400	0.400	0.343
7	0.232	0.257	0.280	0.332	0.344	0.352	0.407	0.406	0.413	0.356	0.359	0.423	0.431	0.379
8	0.232	0.256	0.281	0.352	0.367	0.367	0.422	0.426	0.447	0.378	0.377	0.446	0.461	0.358
9	0.232	0.255	0.282	0.372	0.390	0.382	0.438	0.446	0.440	0.400	0.396	0.470	0.461	0.334
10	0.232	0.254	0.281	0.373	0.414	0.396	0.453	0.466	0.434	0.422	0.414	0.493	0.453	0.309
11	0.233	0.254	0.280	0.369	0.437	0.411	0.468	0.485	0.427	0.417	0.433	0.516	0.445	0.285
12	0.233	0.253	0.278	0.365	0.435	0.426	0.484	0.505	0.421	0.411	0.431	0.507	0.437	0.260
13	0.233	0.252	0.276	0.361	0.429	0.441	0.499	0.525	0.414	0.406	0.427	0.497	0.428	0.236
14	0.233	0.252	0.275	0.357	0.424	0.449	0.515	0.520	0.407	0.401	0.424	0.487	0.420	0.211
15	0.233	0.251	0.273	0.352	0.418	0.444	0.527	0.511	0.401	0.396	0.420	0.478	0.412	0.187
16	0.233	0.250	0.271	0.348	0.412	0.439	0.519	0.503	0.394	0.390	0.417	0.468	0.403	0.162
17	0.234	0.249	0.270	0.344	0.406	0.434	0.512	0.494	0.387	0.385	0.413	0.459	0.395	0.138
18	0.234	0.249	0.268	0.340	0.400	0.429	0.504	0.486	0.380	0.380	0.410	0.449	0.387	0.114
19	0.234	0.248	0.267	0.336	0.395	0.424	0.496	0.477	0.373	0.374	0.406	0.440	0.377	0.089
20	0.234	0.247	0.265	0.332	0.389	0.419	0.488	0.469	0.365	0.369	0.403	0.430	0.362	0.077
21	0.234	0.247	0.263	0.328	0.383	0.414	0.481	0.460	0.358	0.364	0.399	0.421	0.347	0.081
22	0.235	0.246	0.262	0.324	0.377	0.410	0.473	0.452	0.350	0.359	0.396	0.411	0.332	0.086
23	0.235	0.245	0.260	0.320	0.372	0.405	0.465	0.443	0.343	0.346	0.392	0.402	0.317	0.090
24	0.235	0.244	0.259	0.316	0.366	0.400	0.458	0.435	0.336	0.328	0.389	0.392	0.303	0.094
25	0.235	0.244	0.257	0.312	0.360	0.395	0.450	0.426	0.328	0.309	0.385	0.382	0.288	0.099

Table 5: Best fitting η estimates for metal-poor stars.

Z	M_{RR} [a]	Age(Gyr) [b]	M_{RG} [c]	ΔM [d]	η
0.0001	0.760	12	0.852	0.092	0.3 – 0.4
0.0001	0.760	14	0.816	0.056	< 0.3
0.0001	0.760	16	0.788	0.028	< 0.3
0.0004	0.710	12	0.862	0.152	0.5
0.0004	0.710	14	0.826	0.116	0.3 – 0.5
0.0004	0.710	16	0.796	0.086	< 0.3

[a] Evolutionary mass of RR Lyrae type-d variables from Yi et al. (1993).

[b] Because of uncertainties, three ages have been chosen for the clusters, M15 and M3.

[c] Mass of red giants at the tip of the RGB, adopted from the Yale Isochrones 1996.

[d] $\Delta M \equiv M_{RG} - M_{RR}$

Table 6: The η suggested by hydrodynamical models.

Z	suggested η
0.0002	0.17 – 0.25
0.002	0.22 – 0.33
0.006	0.33 – 0.50
0.02	1.0

REFERENCES

Aaronson, M., & Mould, J. 1982, ApJS, 48, 161

Allen, C. W. 1976, in Astrophysical Quantities (The Athlone Press: London), 202

Bailyn, C. D. 1995, Ann. Rev. A. & Ap, 33, 133

Bertola, F., Burstein, D., Buson, L. M., & Renzini, A. 1993, ApJ, 403, 577

Blöcker, T., & Schönberner, D. 1990, A&A, 240, L11

Bowen, G. H., & Willson, L. A. 1991, ApJ, 371, L53

Bressan, A., Chiosi, C., & Fagotto, F. 1994, ApJS, 94, 63

Brown, T. H., Ferguson, H. C., & Davidsen, A. F. 1995, ApJ, 454, L15

Brown, T. M., Ferguson, H. C., Davidsen, A. F., & Dorman, B. 1997, preprint

Bruzual, A. G., & Charlot, S. 1993, ApJ, 405, 538

Burstein, D., Bertola, F., Buson, L. M., Faber, S. M., & Lauer, T. R. 1988, ApJ, 328, 440

Buser, R., & Kurucz, R. L. 1992, A&A, 264, 557

Buzzoni, A. 1995, ApJS, 98, 69

Cacciari, C., Fusi Pecci, F., Bragaglia, A., & Buzzoni, A. 1991, A&A, 301, 684

Castellani, M., & Castellani, V. 1993, ApJ, 407, 649

Castellani, M., & Tornambé, A. 1991, ApJ, 381, 393

Catelan, M. 1993, A&ASuppl., 98, 547

Chaboyer, B., Demarque, P., & Sarajedini, A. 1996, ApJ, 459, 558

Charlot, S., Worthey, G., & Bressan, A. 1996, ApJ, 457, 625

Clement, C. M., Kinman, T. D., & Suntzeff, N. B. 1991, ApJ, 372, 273

Code, A. D., & Welch, G. A. 1979, ApJ, 228, 95

Cole, P. W., & Deupree, R. G. 1980, ApJ, 239, 284

Cole, P. W., Demarque, P. & Deupree, R. G. 1985, ApJ, 291, 291

Cox, A. N. 1991, ApJ, 381, L71

de Boer, K. S., Tucholke, H.-J., & Schmidt, J. H. K. 1997, A&A, 317, L23

Demarque, P., Chaboyer, B., Guenther, D., Pinsonneault, L., Pinsonneault, M., & Yi, S. 1996, The Yale Isochrones 1996

Demarque, P. & Mengel, J. G. 1971 ApJ, 164, 469

Demarque, P., & Pinsonneault, M. H. 1988, in Progress & Opportunities in Southern Hemisphere Optical Astronomy, eds. V. M. Blanco & M. M. Phillips (San Francisco: ASP), 371

Dixon, W. V. D., Davidsen, A. F., Dorman, B., & Ferguson, H. 1996, AJ, in press

Dorman, B., Rood, R. T., & O'Connell, R. 1993, ApJ, 419, 596

Dorman, B., O'Connell, R., & Rood, R. T. 1995, ApJ, 442, 105

Dupree, A. K. 1986, ARA&A, 24, 377

D'Cruz, N. L., Dorman, B., Rood, R. T., & O'Connell, R. 1996, ApJ, 466, 359

Faber. S. M. 1972, A&A, 20, 361

Faber. S. M. 1983, Highlights Astr., 6, 165

Fagotto, F., Bressan, A., Bertelli, G., & Chiosi, C. 1994, A&AS, 105, 39

Fanelli, M. N., O'Connell, R. W., & Thuan, T. X. 1987, ApJ, 321, 768

Fanelli, M. N., O'Connell, R. W., Burstein, D., & Wu, C.-C. 1992, ApJS, 82, 197

Ferguson, H. C., & Davidsen, A. F. 1993, ApJ, 408, 92

Ferraro, F. R., Clementi, G., Fusi Pecci, F., Sortino, R., & Buonanno, R. 1992, MNRAS, 256, 391

Fusi Pecci, F., Ferraro, F. R., Bellazzini, M., Djorgovski, S., Piotto, G., & Buonanno, R. 1993, AJ, 105, 1145

Greggio, L., & Renzini, A. 1990, ApJ, 364, 35

Gunn, J. E., & Stryker, L. L. 1983, ApJS, 52, 121

Gunn, J. E., Stryker, L. L., & Tinsley, B. M. 1981, ApJ, 249, 48

Gustafsson, B., & Jørgensen, U. G. 1994, Astron. Astrophys. Rev., 6, 19

Hayashi, C., Hoshi, R., & Sugimoto, D. 1962, Prog. Theor. Phys. Suppl., 22, 1

Horch, E., Demarque, P., & Pinsonneault, M. 1992, ApJ, 388, L53

Hubeny, I. 1988, Computer Physics Communications, 52, 103

Jørgensen, U. G., & Thejll, P. 1993, A&A, 272, 255

Jørgensen, U. G., & Thejll, P. 1993, ApJ, 411, L67

Kaluzny, J., & Udalski, A. 1992, AcA, 42, 29

Kaluzny, J., & Rucinski, S. M. 1995, A&A, 114, 1

Kirkpatrick, J. D., Kelly, D. M., Rieke, G. H., Liebert, J., Allard, F., & Wehrse, R. 1993, ApJ, 402, 643

Kovacs, G., Buchler, J. R., & Marom, A. 1991, A&A, 252, 27

Kudritzki, R. P., & Reimers, D. 1978, A&A, 70, 227

Kurucz, R. 1992, in The Stellar Population in Galaxies, ed. B. Barbuy & A. Renzini (Dordrecht: Reidel), 225

Larson, R. B. 1992, MNRAS, 256, 641

Larson, R. B. 1995, MNRAS, 272, 213

Lee, Y.-W., & Demarque, P. 1990, ApJS, 73, 709

Lee, Y.-W., Demarque, P., & Zinn, R. 1990, ApJ, 350, 155

Lee, Y.-W., Demarque, P., & Zinn, R. 1994, ApJ, 423, 248

Liebert, J., Saffer, R. A., & Green, E. M. 1994, AJ, 107, 1408

Maeder, A. 1991, QJRAS, 32, 217

Magris, G. C., & Bruzual, A. G. 1993, ApJ, 417, 102

McClure, R. D., & van den Bergh, S. 1968, AJ, 73, 313

Miller, G. E., & Scalo, J. M. 1979, ApJS, 41, 513

Moehler, S., Heber, U., & de Boer, K. S. 1995, A&A, 294, 65

Morossi, C., Franchini, M., Malagnini, M. L., Kurucz, R. L., & Buser, R. 1993, A&A, 277, 173

Mould, J., & Aaronson, M. 1982, ApJ, 263, 629

Nesci, R., & Perola, G. C. 1985, A&A, 145, 296

O'Connell, R. W. 1976, ApJ, 206, 370

O'Connell, R. W. 1987, in Stellar Populations, ed. C. A. Norman, A. Renzini, & M. Tosi (Cambridge: Cambridge University Press), 167

O'Connell, R. W. et al. 1992, ApJ, 395, L45

Park, J.-H., & Lee, Y.-W. 1997, ApJ, 476, in press

Petersen, J. O. 1973, A&A, 27, 89

Pickles, A. J. 1985a, ApJS, 59, 33

Pickles, A. J. 1985b, ApJ, 296, 340

Refsdal, S., & Weigert, A. 1970, A&A, 6, 426

Reimers, D. 1975, Mém. Soc. Roy. Sci. Liège, 6th Ser., 8, 369

Renzini, A. 1981, in Physical Processes in Red Giants, ed. I. Iben & A. Renzini (Dordrecht: Reidel), 431

Rood, R. T. 1973, ApJ, 184, 815

Rood, R. T. 1990, in The Confrontation between Stellar Pulsation and Evolution, ed. C. Cacciari & G. Clementi (San Francisco: ASP), 11

Salpeter E. E. 1955, ApJ, 121, 161

Schönberner, D. 1979, A&A, 79, 108

Schönberner, D. 1983, ApJ, 272, 708

Silva, D. R., & Cornell, M. E. 1992, ApJS, 81, 865

Smith, G., & Norris, J. 1983, ApJ, 264, 215

Spinrad, H., & Taylor, B. 1971, ApJS, 22, 445

Sweigart, A. V. 1987, ApJS, 65, 95

Sweigart, A. V., Mengel, J. G., & Demarque, P. 1974, A&A, 30, 13

Tantalo, R., Chiosi, C., Bressan, A., & Fagotto, F. 1996, A&A, 311,361

Tinsley, B. M. 1968, ApJ, 151, 547

Tinsley, B. M. 1972, A&A, 20, 383

Tinsley, B. M. 1980, Fund. Cosmic Phys., 5, 287

Tomasko, M. G. 1970, ApJ, 162, 125

Walker, A. R. 1992, PASP, 104, 1063

Willson, L. A., Bowen, G. H., & Struck, C. 1996, in From Stars to Galaxies, ed. C. Leitherer, U. Fritze-v. Alvensleben, & J. Huchra (ASP), 197

Yi, S. 1996, Ph. D. Thesis, Yale University

Yi, S., Afshari, E., Demarque, P., & Oemler, A. Jr. 1995, ApJ, 453, L69

Yi, S., Demarque, P., & Kim, Y.-C. 1997, ApJ, 482, 677 (YDK)

Yi, S., Demarque, P., & Oemler, A. Jr. 1997, ApJ, in preparation

Yi, S., Lee, Y.-W., & Demarque, P. 1993, ApJ, 411, L25

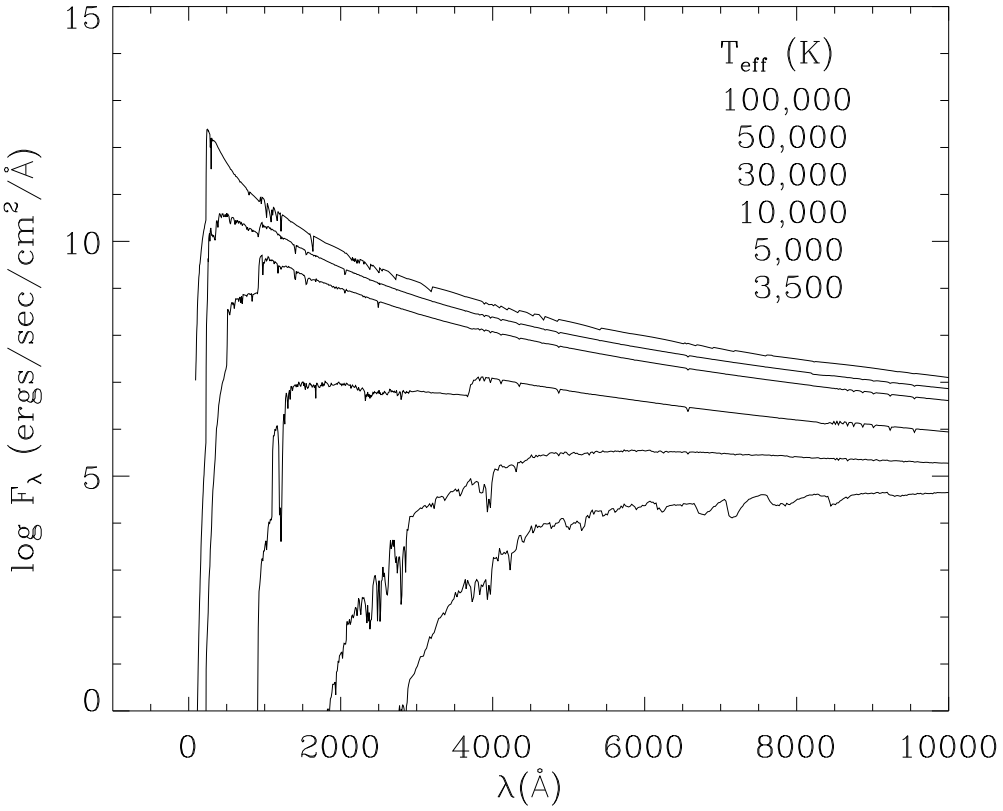

Fig. 1.— Variation of SED as a function of temperature for $Z = Z_{\odot}$ and $\log g = 5.0$. From the top, $T_{\rm eff}$ = 100,000, 50,000, 30,000, 10,000, 5,000, & 3,500 K. Model spectra of $T_{\rm eff} > 50{,}000$ have been constructed using Hubeny's spectral synthesis code while others are all from the Kurucz spectral library.

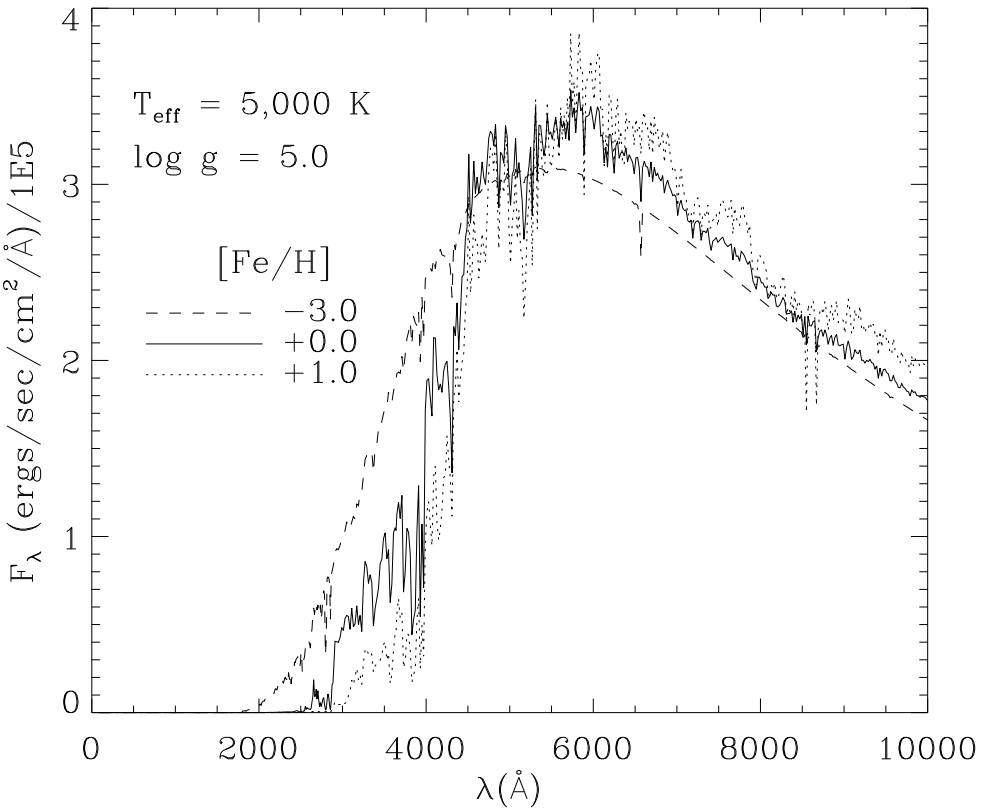

Fig. 2.— Variation of SED as a function of metallicity for $[Fe/H] = -3$, 0, and +1, all for $T_{\rm eff} =$ 5,000 K and $\log g = 5.0$.

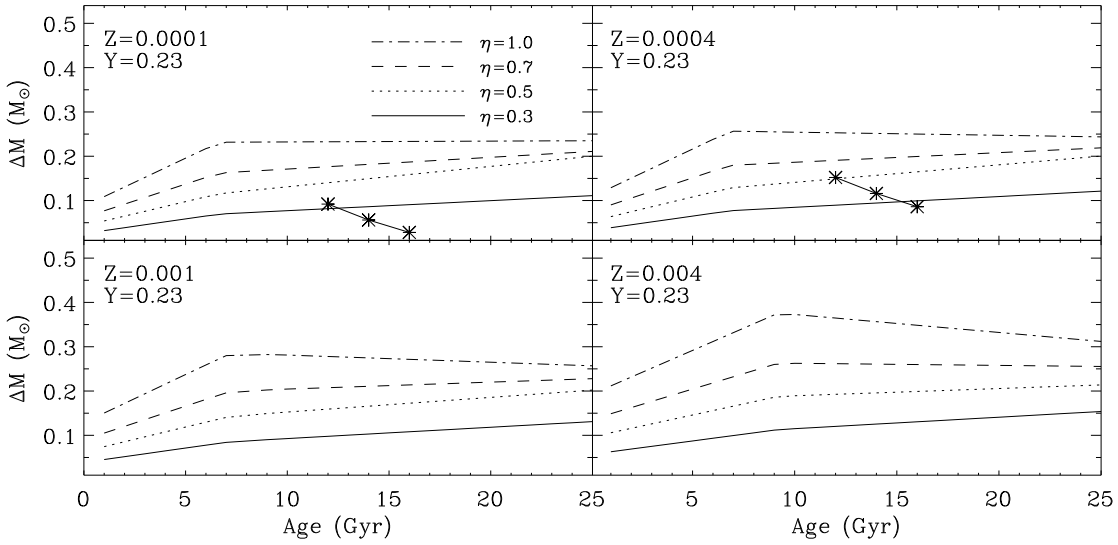

Fig. 3.— Mass loss estimates for metal-poor stars based on Reimers' formula with a variety of efficiency parameters η. Estimation has been made using stellar evolutionary tracks that were used to construct the Yale Isochrones 1996 . In the top two panels, the lines with asterisks are from the measured mass of the RR Lyrae stars, M_{RR}, in the globular clusters assuming the age range of 12 – 16 Gyrs as shown in Table 5. The M_{RR} for $Z = 0.0001$ and $Z = 0.0004$ are best reproduced by $\eta \leq 0.3$ and $\eta \approx 0.3$ – 0.5, respectively.

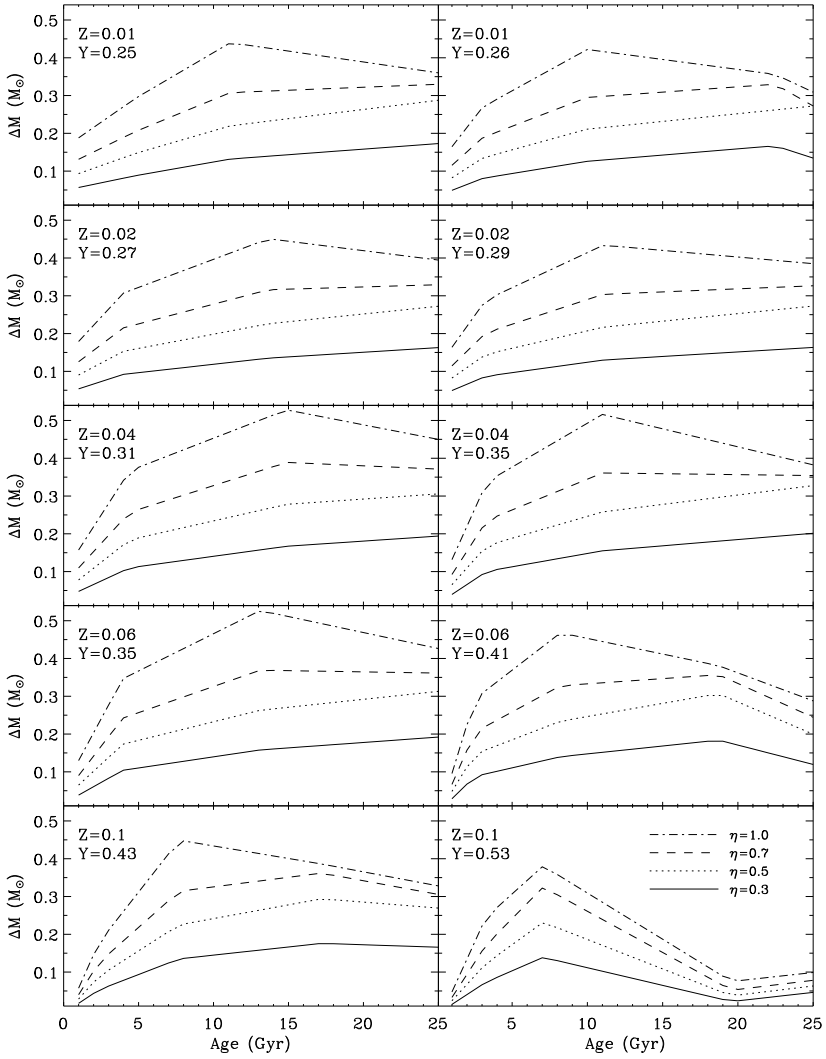

Fig. 4.— Same as Figure 3 but for metal-rich stars. The left and right panels are for $\Delta Y/\Delta Z =$ 2 and 3, respectively. Mass loss as a function of age cannot increase indefinitely as η increases because the mass of the red giants and their core mass also depend on age and metallicity. After a critical age, mass loss decreases for this reason.

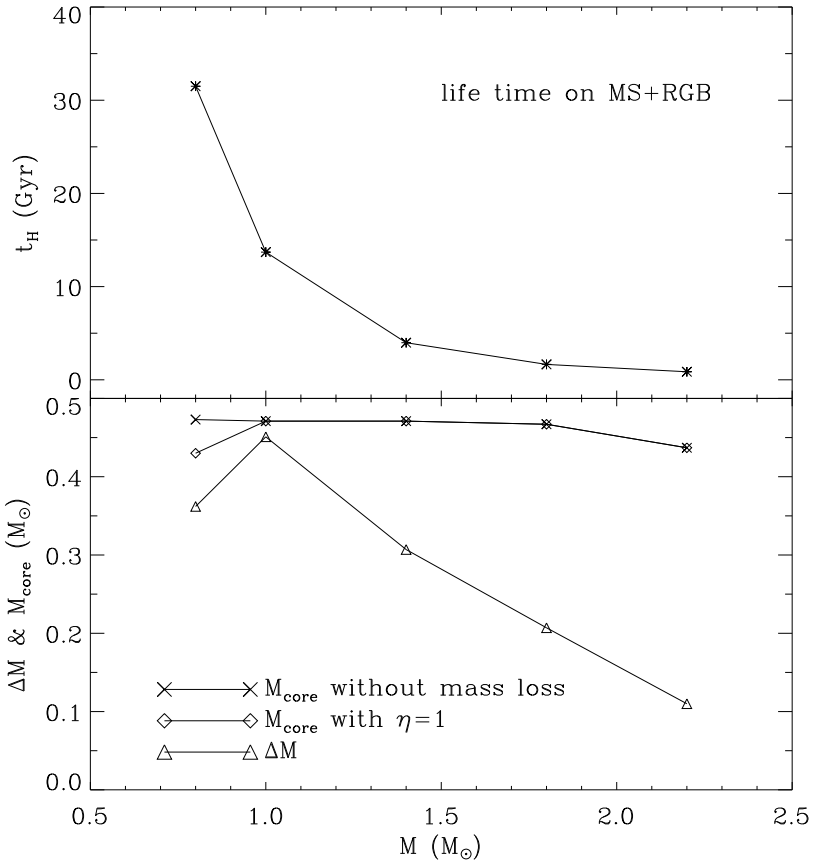

Fig. 5.— Lifetime on the MS and RGB, t_H (upper panel), the core mass at the tip of the RGB, M_{core} , and the mass loss, ΔM (lower panel), as a function of initial mass M for $Z = Z_\odot$. ΔM increases rapidly as M decreases because t_H increases as M decreases. Below a certain mass, $M \approx 1.0$ in case of $Z = Z_\odot$, however, ΔM decreases as M decreases because M_{core} grows too fast to allow more mass loss to occur. A different mass loss efficiency η, therefore, leads to a different final core mass.

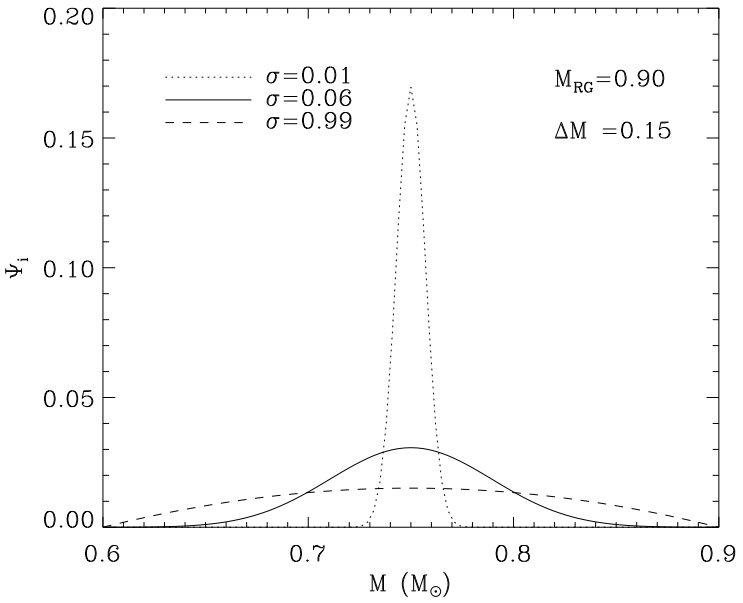

Fig. 6.— Mass distribution functions assumed in this population synthesis. The model with $\sigma = 0.06\ M_\odot$ reproduces the width of the HB of Galactic globular clusters (Lee et al. 1990). The models with $\sigma = 0.01$ and 0.99 are the two extreme assumptions that represent a pseudo-delta function and a pseudo-constant function for mass distribution.

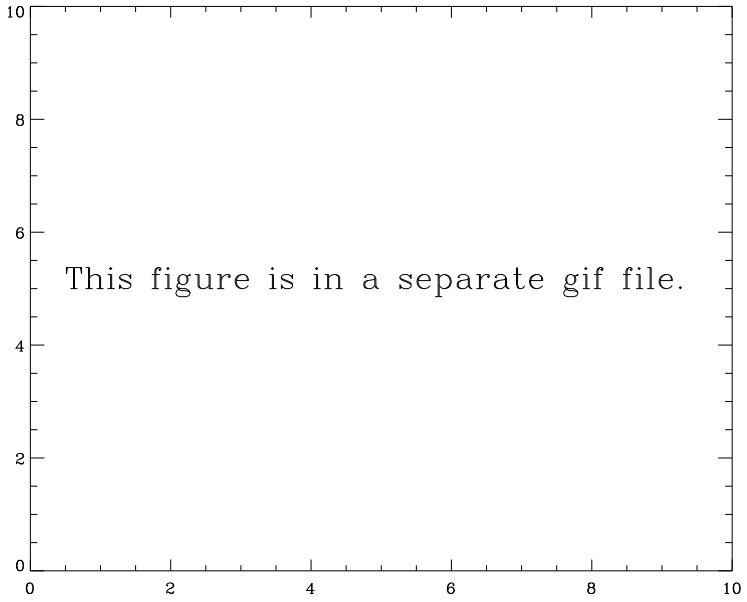

Fig. 7.— Model CMD for low metallicity as a function of age and metallicity. The synthetic HBs are based on the assumption of (η, x, σ) = (1.0, 1.35, 0.06). Note that the HB becomes hotter as age increases. A larger circle denotes a larger number of stars, where the total initial mass of the model galaxy is 10^{12} $M_{\odot}$. It is important to note that these models are based on $\eta = 1.0$. We think that this value is adequate only for metal-rich stars and is much higher than the estimated value (≈ 0.3 – 0.5) for metal-poor stars. As a result, the 15 Gyr old $Z = 0.004$ model with $\eta =$ 1.0 (bottom right panel) contains too many blue HB stars compared to 47 Tuc. Nevertheless, η has been kept the same for all models of different ages and metallicities in Figures 7 – 12 in order to see only the effect of age and metallicity. The brightest PAGB track (in 15 Gyr-old models) is the Kiel group 0.598 $M_{\odot}$ model, and the second and third are their 0.565 and 0.546 $M_{\odot}$ models, respectively. The fourth brightest horizontally crossing track is for the stars that do not have a sufficiently large mass to experience helium core flash (Sweigart et al. 1974; see text).

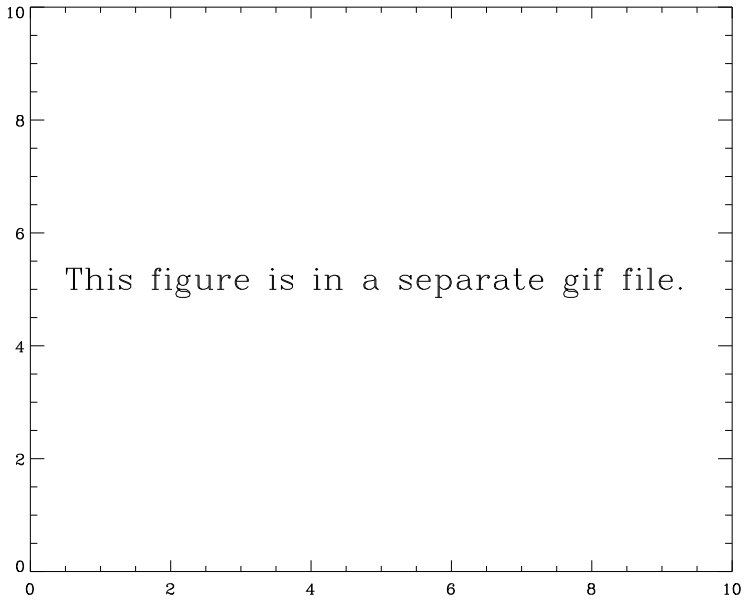

Fig. 8.— Same as Figure 7, but for metal-rich populations of $Z \geq 0.01$ and $\Delta Y/\Delta Z = 2$. Note that metal-rich models have many UV-bright (slow blue phase) stars.

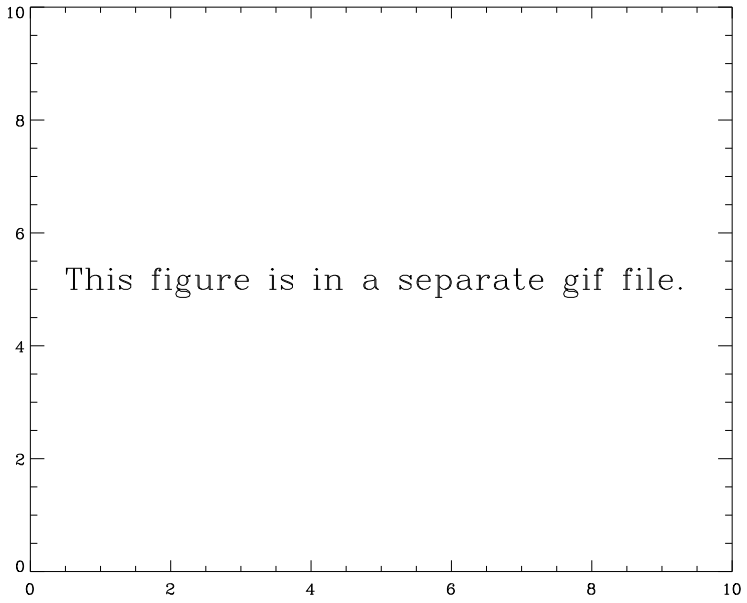

Fig. 9.— Same as Figure 7, but for metal-rich populations of $Z \geq 0.01$ and $\Delta Y/\Delta Z = 3$. The UV-bright phase, the SBP, is even more conspicuous than the case of $\Delta Y/\Delta Z = 2$ in Figure 8.

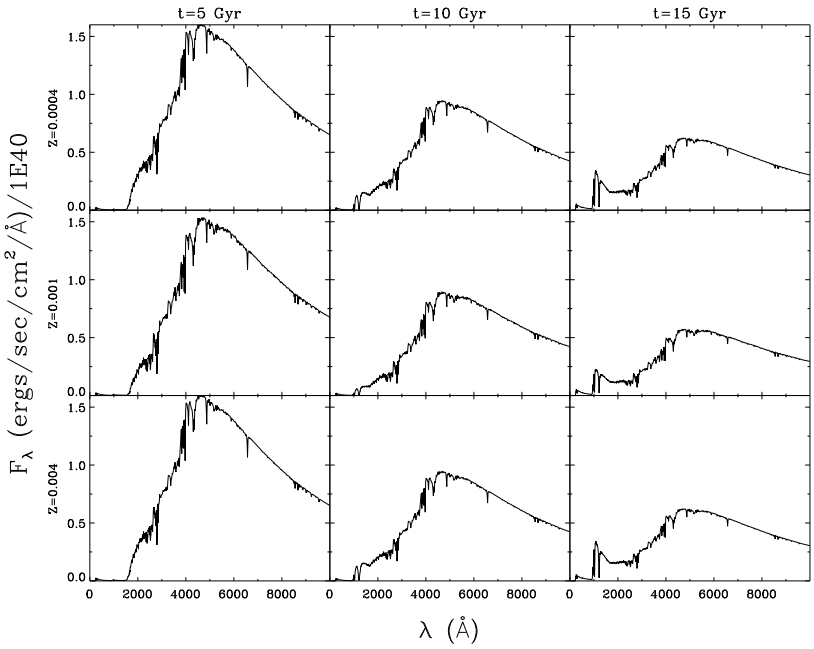

Fig. 10.— Model SED for low metallicity as a function of age and metallicity. These models are based on the model CMDs shown in Figure 7. A noticeable "UV upturn" appears at a large age. Once again, keep in mind that the metal-poor models overproduce UV flux almost certainly because $\eta = 1.0$, a factor of 2 – 3 overestimation for metal-poor stars, has been used in this figure. The y-axis is in an arbitrary scale.

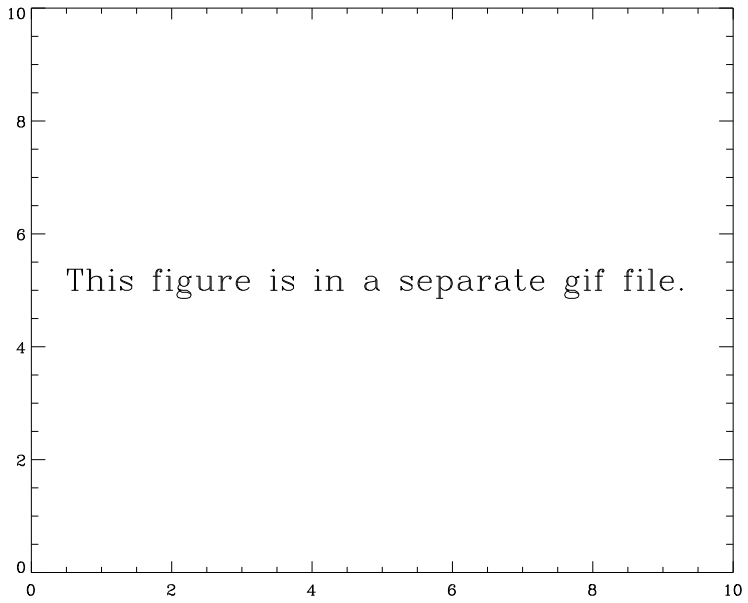

Fig. 11.— Same as Figure 10, but for $Z \geq 0.01$ and $\Delta Y/\Delta Z = 2$. The far-UV flux relative to the near-UV flux is generally higher than the metal-poor models in Figure 10.

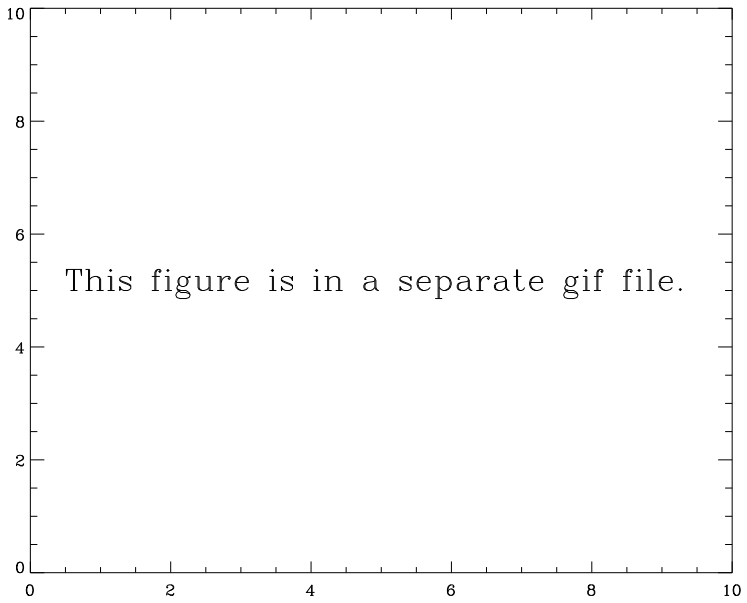

Fig. 12.— Same as Figure 11, but for $\Delta Y/\Delta Z = 3$. A strong UV flux develops more quickly when $\Delta Y/\Delta Z$ is higher because the UV-bright shell helium-burning phase (the SBP) is more significant when helium abundance is higher (Dorman et al. 1993; YDK).

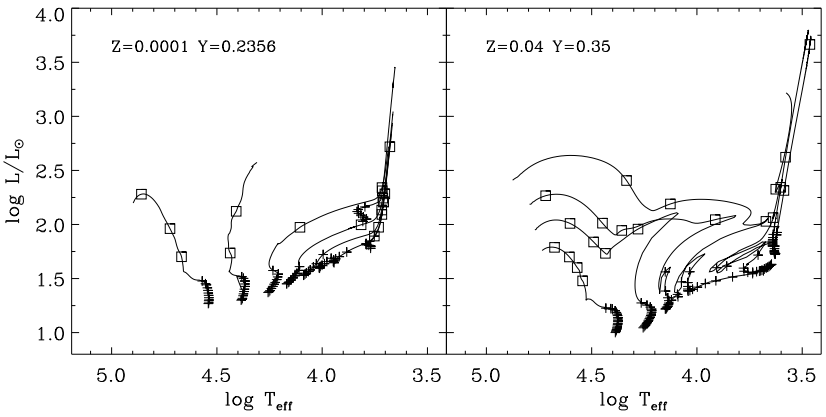

Fig. 13.— The definitions of central and shell helium-burning stages. The crosses and squares are for central and shell helium-burning stages, respectively. All symbols denote time interval of 10 Myr.

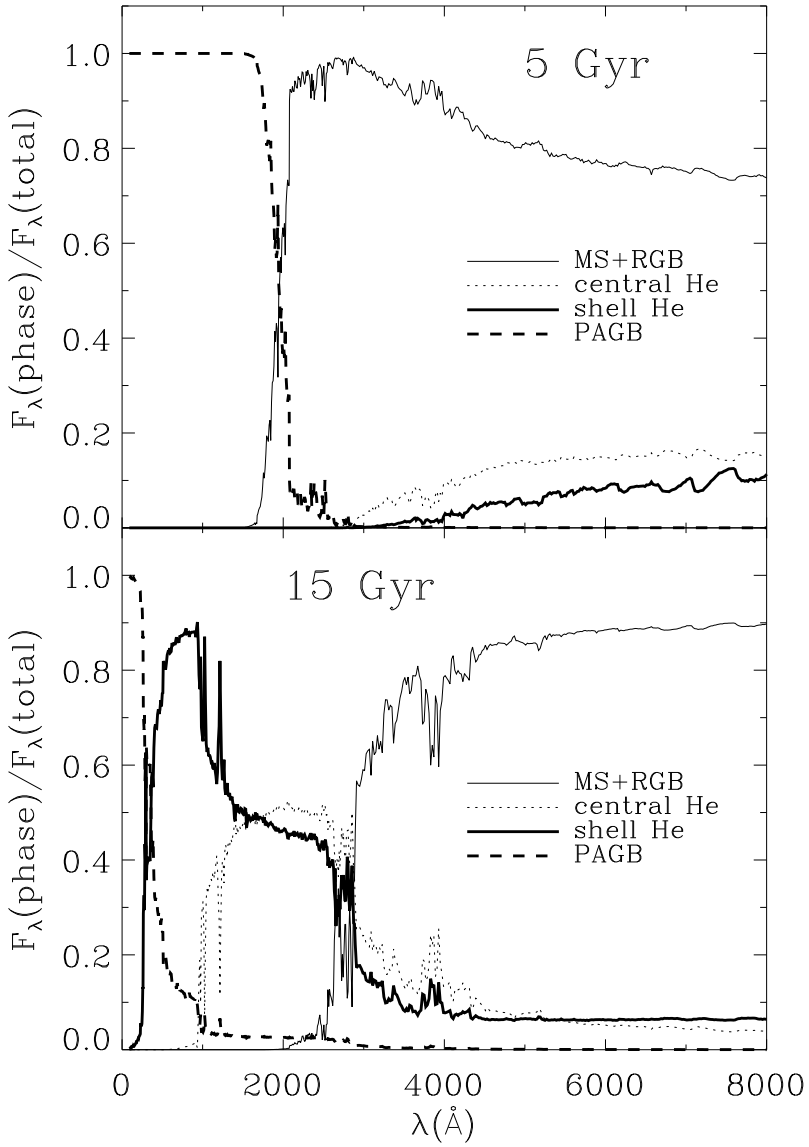

Fig. 14.— Light contribution from various evolutionary stages at different ages. The upper and the lower panels are for 5 and 15 Gyrs old models, respectively, both with (Z, Y, η, x, σ) = (0.02, 0.29, 1.0, 1.35, 0.06). At an early age, the most UV light comes from PAGB stars, while the UV flux is almost negligible, as seen in Figure 12. The lower panel shows that much of the UV light at 15 Gyr, especially in the far-UV, originates from shell helium-burning (evolved HB) stars in the UV-bright phase (SBP) discussed in YDK.

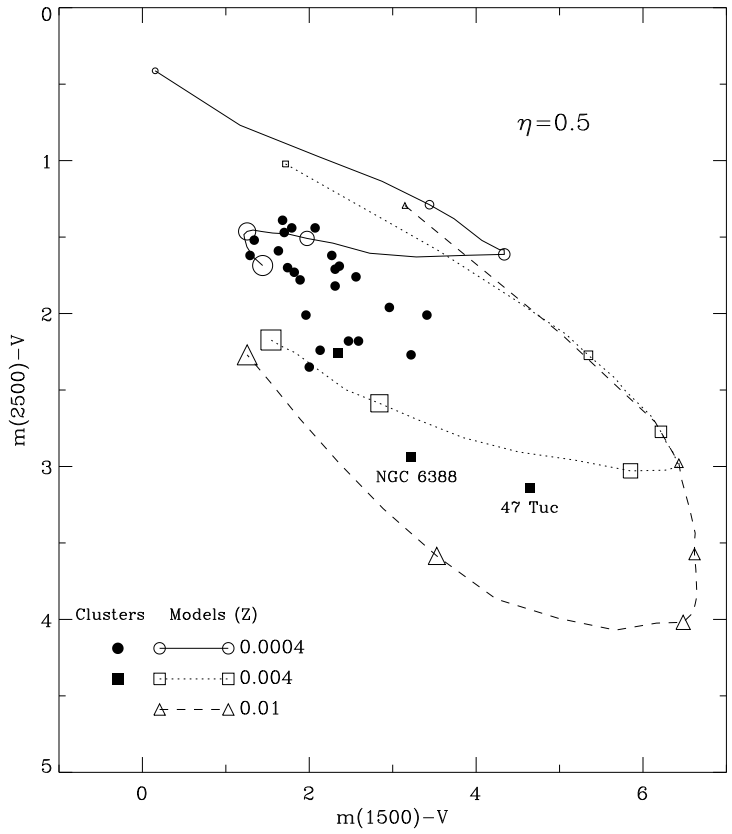

Fig. 15.— Effects of age and metallicity on the model two-color diagram, m(1500)-V vs m(2500)-V. Each line is for one metallicity but covering 1 – 25 Gyrs of age. From the smallest symbol to the largest, symbols denote 1, 5, 10, 15, 20, and 25 Gyr old models. In order to show only the effects of age and metallicity, other parameters are fixed, i.e. (η, σ, x) = (0.5, 0.06, 1.35). The model colors are defined in the text, and the cluster data are from Table 1 of Dorman et al. (1995). Filled circles and filled squares are metal-poor cluster data ($Z < 0.002$) and metal-rich cluster data ($Z \geq 0.002$), respectively. Most data points are matched by the models with the age derived from the MS turn-off in the CMD (approximately 15 Gyr). Because of the opacity effect, the more metal-rich, the redder the UV-to-V colors. The issue about the true η is discussed in Section 4.2.

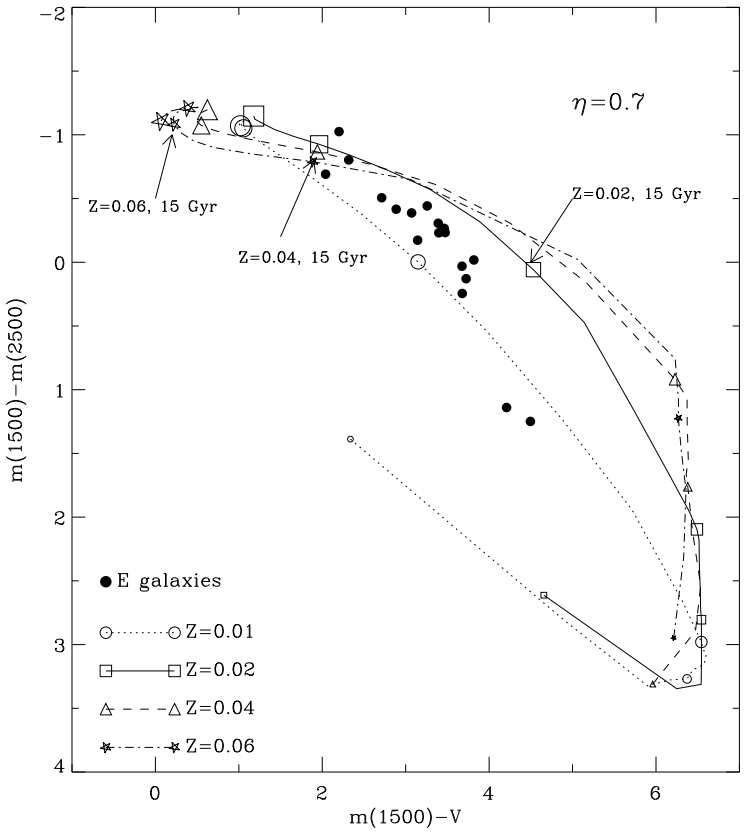

Fig. 16.— Same as Figure 15, but for metal-rich systems in the m(1500)-V vs m(1500)-m(2500) diagram. In order to show only the effects of age and metallicity, other parameters are fixed, i.e. (η, σ, x) = (0.7, 0.06, 1.35). The galaxy data are from Table 2 of Dorman et al. (1995). If the majority of stars in elliptical galaxies are approximately 1 – 2 $Z_{\odot}$, then the $\eta = 0.7$ models suggest that elliptical galaxies are about 15 Gyrs old.

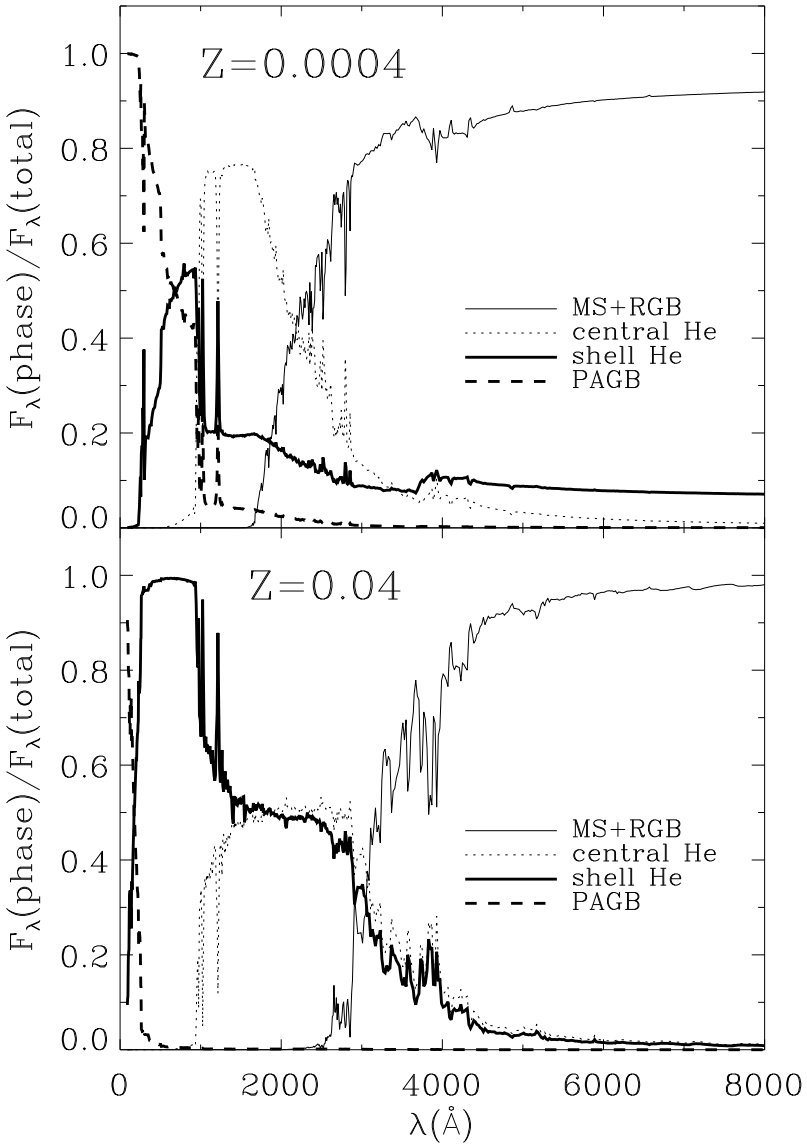

Fig. 17.— Light contribution from various evolutionary stages for different metallicities. The upper and lower panels are for a metal-poor model with (Z, Y) = (0.0004, 0.23), and a metal-rich model with (0.04, 0.35), respectively, both with (age, η, x, σ) = (15 Gyr, 1.0, 1.35, 0.06). Most UV light comes from the central helium-burning stars (HB stars) in the metal-poor model. But, a larger amount of UV light comes from the highly evolved, shell helium-burning stars in the metal-rich case (lower panel) due to the UV-bright phase that is more common in the metal-rich stars.

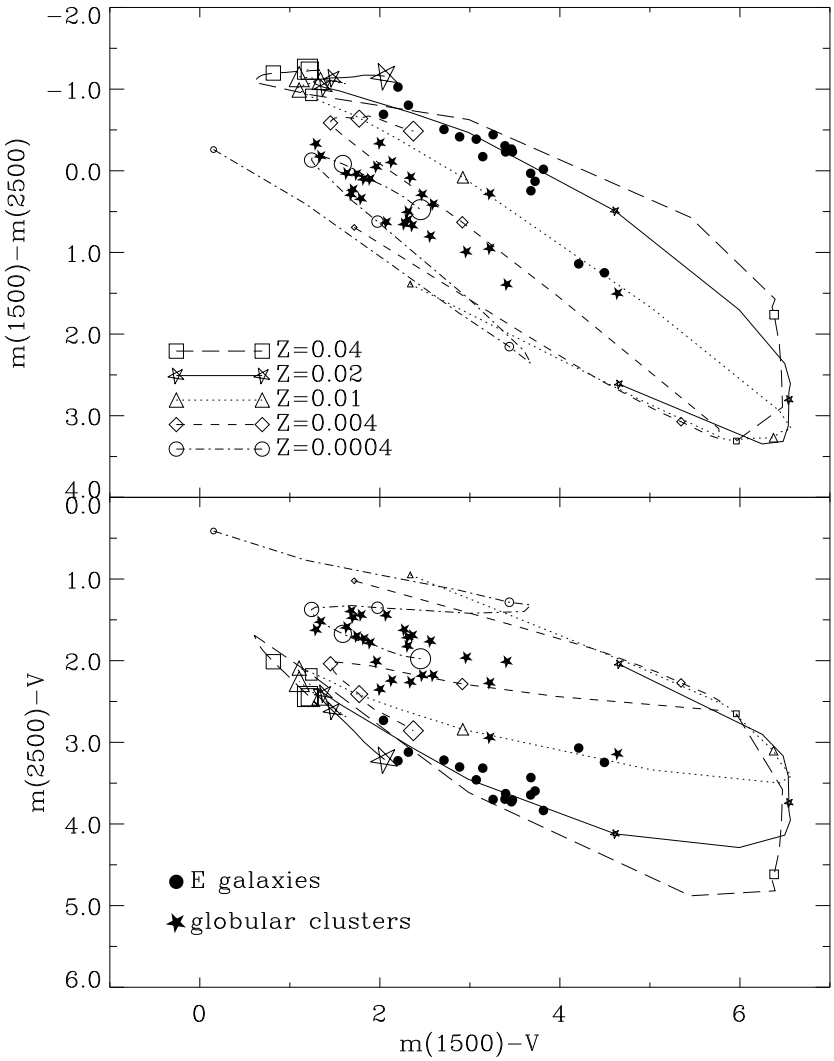

Fig. 18.— Effects of age and metallicity on model two-color diagrams. In order to show only the effects of age and metallicity, other parameters are fixed as ($\Delta Y/\Delta Z$, η, σ, x) = (3.0, 1.0, 0.06, 1.35). If $\eta \approx 0.3$ – 0.5 for metal-poor stars as discussed in the text, the metal-poor models with $\eta = 1.0$ shown in this diagram are generating too much UV flux at a given age. The issue about the true η is discussed in Section 4.2. Note that elliptical galaxies are best matched by metal-rich models whereas metal-poor models reproduce the globular clusters well as normally expected.

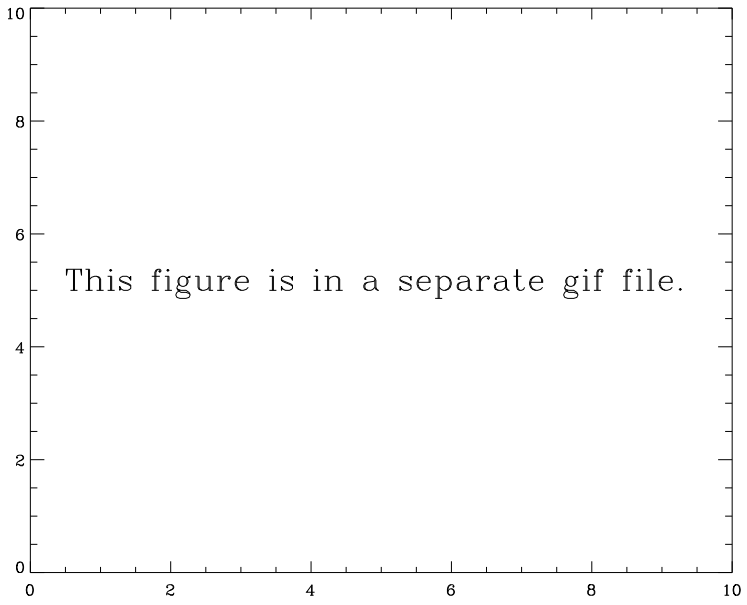

Fig. 19.— Effects of η on model CMDs and SEDs for (Z, Y, age, σ, x) = (0.04, 0.31, 15 Gyr, 0.06, 1.35). F_λ is in arbitrary but consistent unit. It is clear that a higher mass loss efficiency leads to a larger number of hot stars and a higher UV flux. Various studies favor a high η, namely, $\eta \geq 0.7$ for $Z \geq Z_\odot$. If this is true, old, metal-rich galaxies can exhibit a strong UV upturn within a Hubble time.

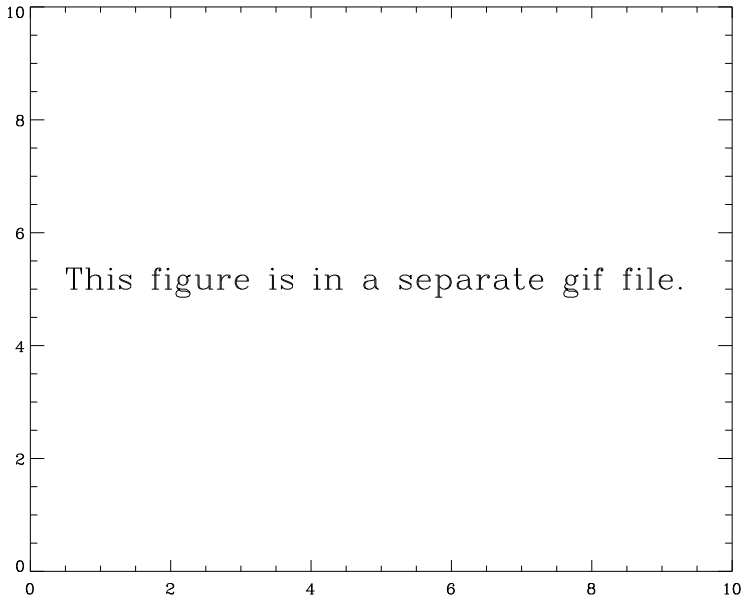

Fig. 20.— Effects of η on model CMDs and SEDs for (Z, Y, age, σ, x) = (0.0004, 0.23, 15 Gyr, 0.06, 1.35). F_λ is in arbitrary but consistent unit. Unless η were as high as unity, an unlikely high value for metal-poor stars, metal-poor populations would fail to produce a strong UV upturn.

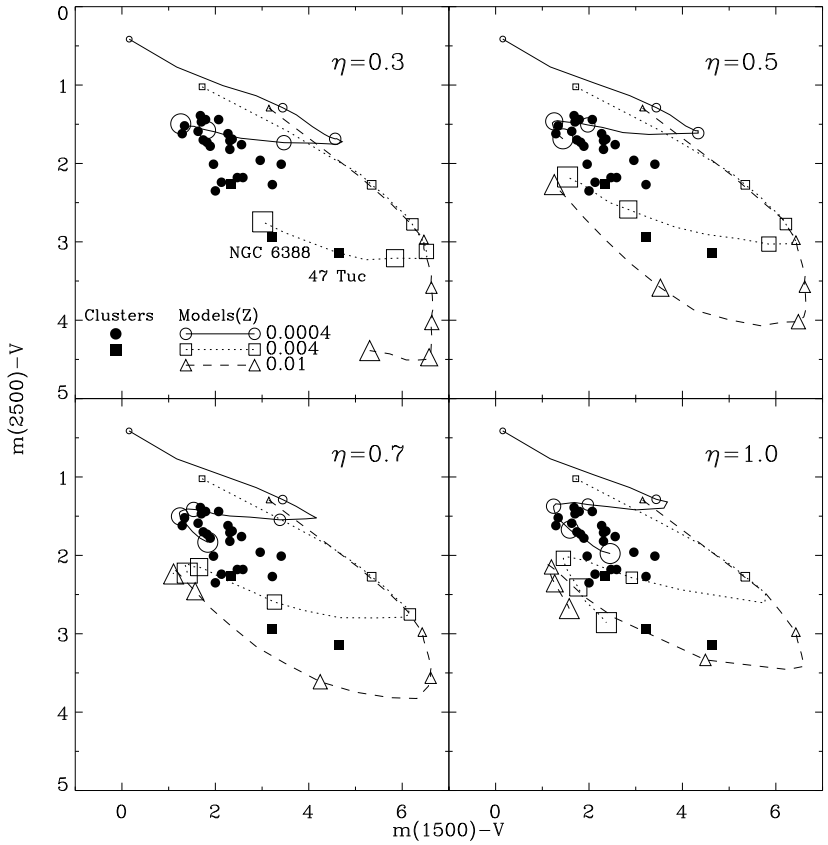

Fig. 21.— Effects of η on model two-color diagrams, m(1500)-V vs m(2500)-V. See the Figure 15 caption for model and symbol descriptions. In order to show only the effects of η, other parameters are fixed, i.e. $(\sigma,\ x) = (0.06,\ 1.35)$. Data for metal-poor globular clusters (filled circles) and relatively metal-rich globular clusters (filled squares) are shown. Note that $\eta = 0.3$ models, which reasonably reproduce the colors of metal-poor clusters, fail to match the colors of the metal-rich globular clusters (e.g. NGC 6388, $Z \approx 0.006$) at an acceptable age; the $\eta = 0.3$ model suggests an age of about 24 Gyrs for NGC 6388.

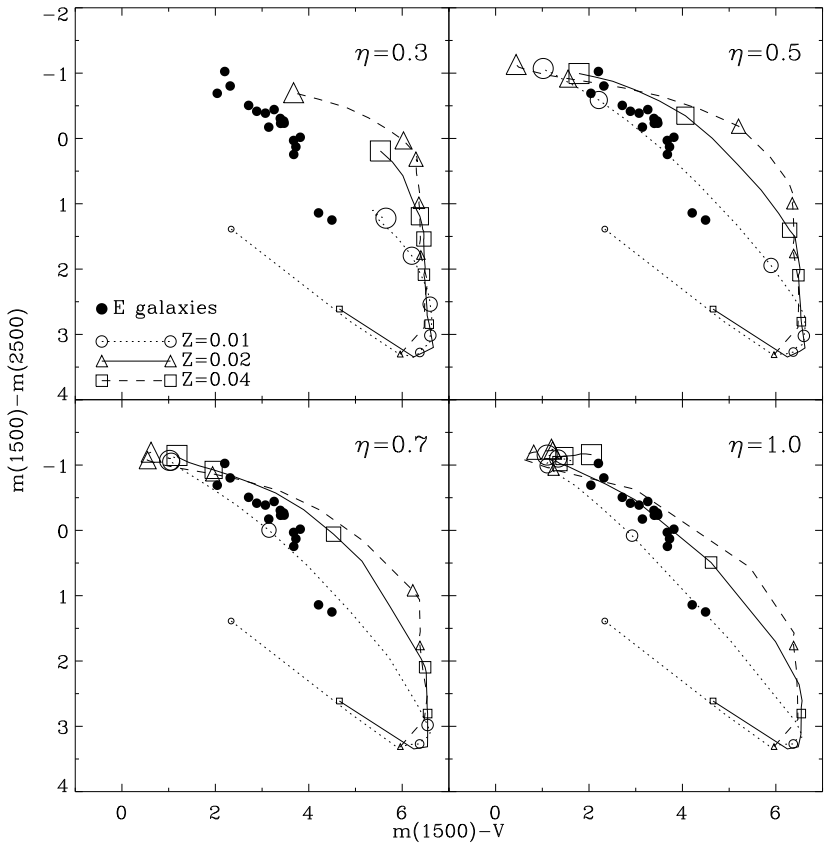

Fig. 22.— Same as Figure 21, but for metal-rich systems on the m(1500)-V vs m(1500)-m(2500) plane. The UV strength of elliptical galaxies cannot be reproduced by low η models. If elliptical galaxies are approximately 15 Gyrs old, this suggests $\eta \gtrsim 0.7$ for metal-rich stars.

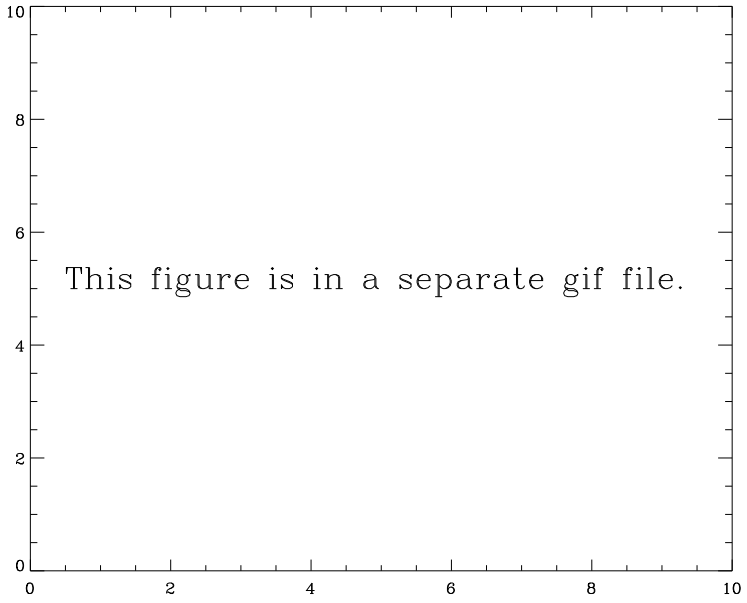

Fig. 23.— An example showing the effects of $\Delta Y/\Delta Z$ on model CMDs and SEDs for (Z, age, η, σ, x) = (0.02, 13 Gyr, 0.06, 1.0, 1.35). F_λ is in arbitrary but consistent unit. A model with a higher $\Delta Y/\Delta Z$ shows a higher UV flux because (1) HB stars with a higher helium abundance, Y, become UV-bright more easily, and (2) stars with a higher Y evolve faster on MS and RGB when $Z \gtrsim Z_\odot$. Thus, a galaxy with a higher $\Delta Y/\Delta Z$ contains a larger number of low-mass (hot) HB stars at a fixed age.

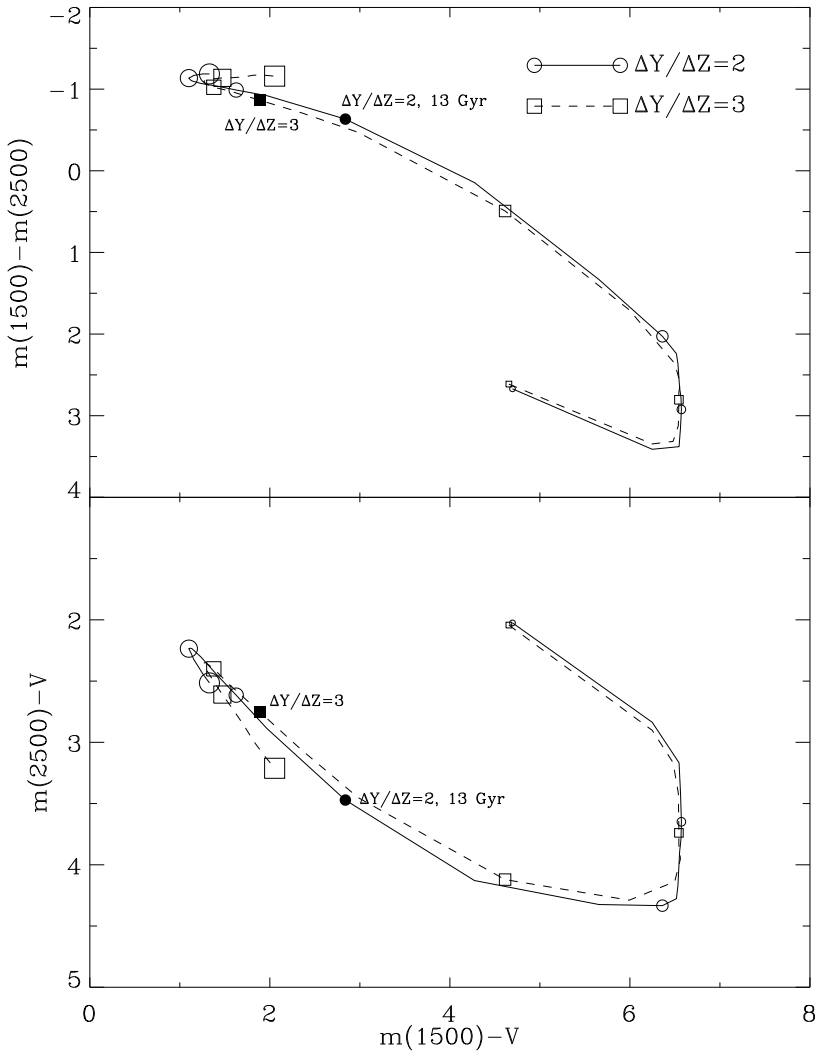

Fig. 24.— Effects of $\Delta Y/\Delta Z$ on model two-color diagrams. Models are for (Z, η, σ, x) = (0.02, 1.0, 0.06, 1.35). Higher-$\Delta Y/\Delta Z$ models generate UV flux more quickly because stars with higher helium abundance evolve faster and because the UV-bright phase of metal-rich HB stars is more significant as helium abundance increases (see YDK). But it is difficult to choose the true $\Delta Y/\Delta Z$ by UV color fitting unless the age is known a priori, because, if $\Delta Y/\Delta Z$ is within the range of 2 – 3, the model sequences of different values of $\Delta Y/\Delta Z$ look very much alike. Symbols are the same as in the Figure 15 except that 13 Gyr-old models (filled symbols) are also marked to be compared with Figure 23.

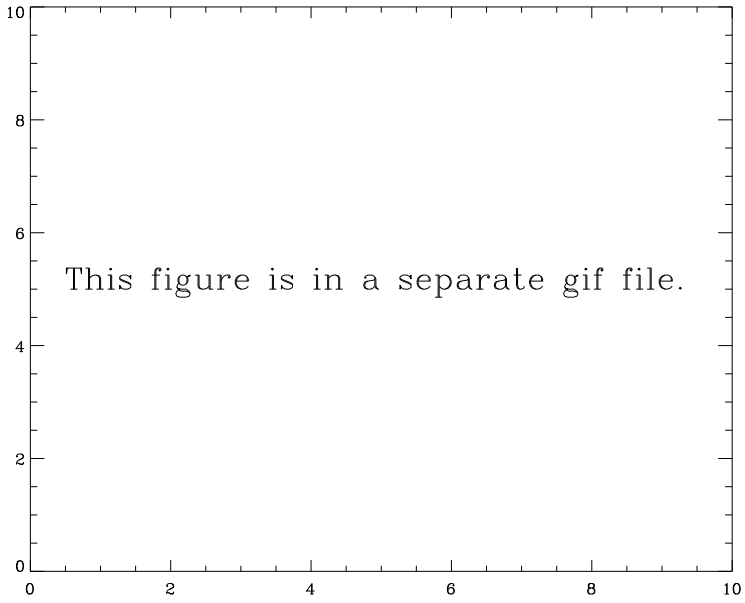

Fig. 25.— Effects of the IMF slope x on model CMDs and SEDs for (Z, Y, age, σ, η) = (0.02, 0.29, 15 Gyr, 0.06, 1.0). F_λ is in arbitrary but consistent unit. A model SED is not very sensitive to the IMF slope x.

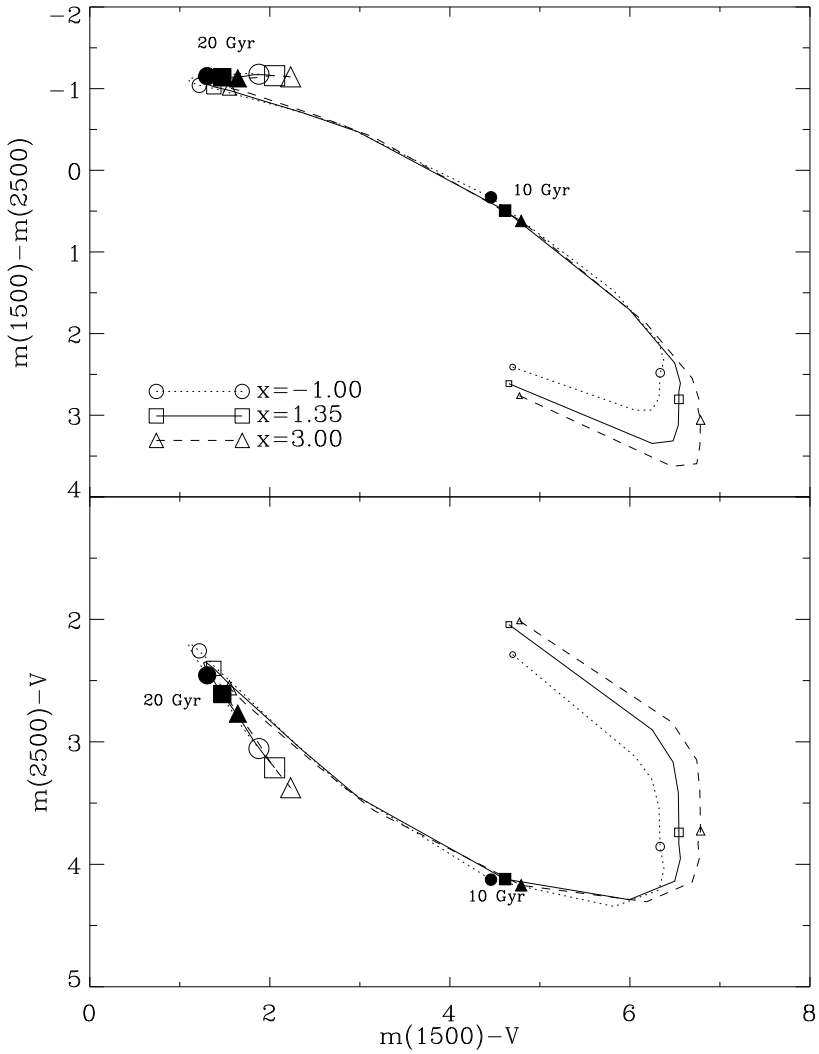

Fig. 26.— Effects of the IMF slope x on model two-color diagrams. Models are for (Z, Y, η, σ) = (0.02, 0.29, 1.0, 0.06). Note that the IMF slope has little effect on the UV-to-V colors. See the Figure 15 caption for details about symbols.

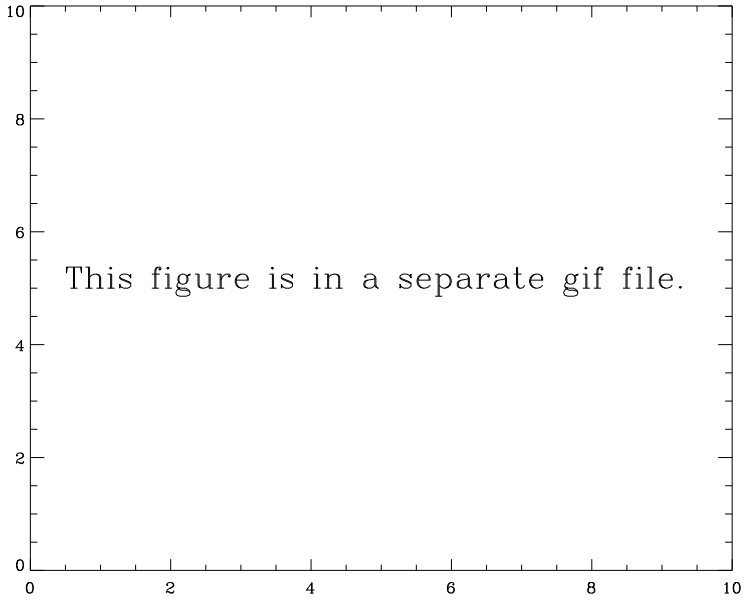

Fig. 27.— Effects of the gaussian mass dispersion factor σ on model CMDs and SEDs for (Z, Y, age, σ, x) = (0.02, 0.29, 10 Gyr, 0.06, 1.35). F_λ is in arbitrary but consistent unit. When a galaxy is so young that a larger fraction of its core helium-burning stars is cool, a larger σ causes a higher UV flux.

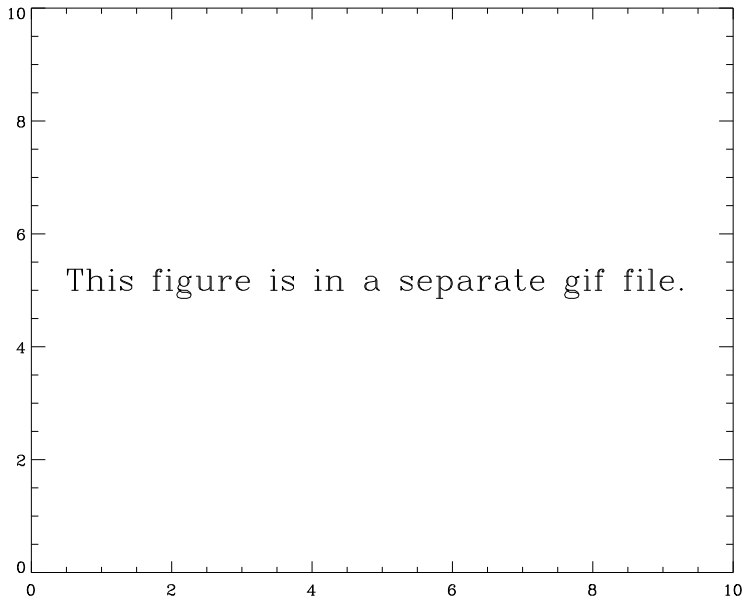

Fig. 28.— Same as Figure 27, but for a 15 Gyr model galaxy. When a galaxy is old enough that a larger fraction of its core helium-burning stars is hot, a larger σ causes a lower UV flux.

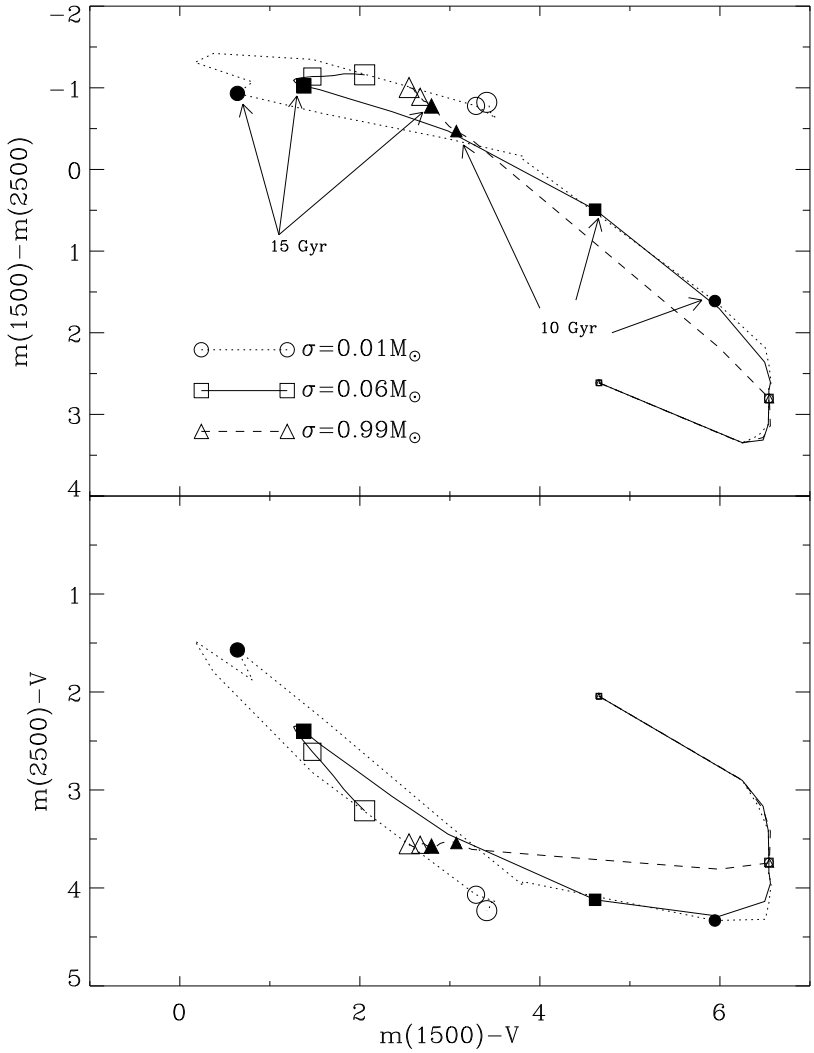

Fig. 29.— Effects of the mass dispersion parameter, σ, on model two-color diagrams. All models are for (Z, Y, η, x) = (0.02, 0.29, 1.0, 1.35). It is clear that the model UV-to-V colors are sensitive to σ which determines the width of the HB. Thus, oversimplistic HB treatments are likely to lead to wrong conclusions. See the Figure 15 caption for details about symbols.

This figure "f7.gif" is available in "gif" format from:

http://arXiv.org/ps/astro-ph/9705173v2

This figure "f8.gif" is available in "gif" format from:

http://arXiv.org/ps/astro-ph/9705173v2

This figure "f9.gif" is available in "gif" format from:

http://arXiv.org/ps/astro-ph/9705173v2

This figure "f11.gif" is available in "gif" format from:

http://arXiv.org/ps/astro-ph/9705173v2

This figure "f12.gif" is available in "gif" format from:

http://arXiv.org/ps/astro-ph/9705173v2

This figure "f19.gif" is available in "gif" format from:

http://arXiv.org/ps/astro-ph/9705173v2

This figure "f20.gif" is available in "gif" format from:

http://arXiv.org/ps/astro-ph/9705173v2

This figure "f23.gif" is available in "gif" format from:

http://arXiv.org/ps/astro-ph/9705173v2

This figure "f25.gif" is available in "gif" format from:

http://arXiv.org/ps/astro-ph/9705173v2

This figure "f27.gif" is available in "gif" format from:

http://arXiv.org/ps/astro-ph/9705173v2

This figure "f28.gif" is available in "gif" format from:

http://arXiv.org/ps/astro-ph/9705173v2